IEEE Access
Multidisciplinary ⋮ Rapid Review ⋮ Open Access Journal

Received 12 September 2025, accepted 13 October 2025, date of publication 27 October 2025, date of current version 31 October 2025.

Digital Object Identifier 10.1109/ACCESS.2025.3626162

RESEARCH ARTICLE

Time Encoding Quantization of Bandlimited and Finite-Rate-of-Innovation Signals

HILA NAAMAN[1], (Member, IEEE), NEIL IRWIN BERNARDO[2], (Member, IEEE), ALEJANDRO COHEN[3], (Senior Member, IEEE), AND YONINA C. ELDAR[1,4], (Fellow, IEEE)

[1]Faculty of Computer Science, the College of Management Academic Studies, Rishon LeZion 7579806, Israel
[2]Electrical and Electronics Engineering Institute, University of the Philippines Diliman, Quezon City 1101, Philippines
[3]Faculty of Electrical and Computer Engineering, Technion—Israel Institute of Technology, Haifa 3200003, Israel
[4]Faculty of Mathematics and Computer Science, Weizmann Institute of Science, Rehovot 7610001, Israel

Corresponding author: Hila Naaman (hilanaaman10@gmail.com)

This work was supported in part by European Research Council (ERC) through European Union's Horizon 2020 Research and Innovation Program under Grant 101000967 and Grant 646804-ERC-COG-BNYQ, in part by European Union (ERC, Stochastic Spiking Wireless Multimodal Sensors Systems (SWIMS)) under Grant 101119062, in part by Israel Science Foundation under Grant 0100101, and in part by the QuantERA Grant Continuously Monitored Quantum Sensors: Smart Tools and Applications (C'MON-QSENS). The work of Neil Irwin Bernardo was supported in part by the Office of the Chancellor of the University of the Philippines Diliman, and in part by the Office of the Vice Chancellor for Research and Development through the Ph.D. Incentive Award 252509.

ABSTRACT This paper studies the impact of quantization in integrate-and-fire time encoding machine (IF-TEM) sampler used for bandlimited (BL) and finite-rate-of-innovation (FRI) signals. An upper bound is derived for the mean squared error (MSE) of IF-TEM sampler and compared against that of classical analog-to-digital converters (ADCs) with uniform sampling and quantization. The interplay between a signal's energy, bandwidth, and peak amplitude is used to identify how the MSE of IF-TEM sampler with quantization is influenced by these parameters. More precisely, the quantization step size of the IF-TEM sampler can be reduced as the maximum frequency of a bandlimited signal or the number of pulses of an FRI signal increases. Leveraging this insight, specific parameter settings are identified for which the quantized IF-TEM sampler achieves an MSE bound that is roughly 8 dB lower than that of a classical ADC with the same number of bits. Experimental results validate the theoretical conclusions.

INDEX TERMS Quantization, time encoding machine, integrate-and-fire, bandlimited signals, finite-rate-of-innovation signals.

I. INTRODUCTION

Sampling and quantization are fundamental topics in signal processing and play a crucial role in numerous applications such as telecommunications, radar, biomedical, and robotic systems [2], [3], [4]. Bandlimited signals are conventionally sampled at or above the rate specified by the Nyquist-Shannon sampling theorem, where the samples are acquired in discrete, equally spaced intervals along time [5], [6]. In these systems, the sampling process is typically coordinated with a main global clock that governs the entire operation. Generally, such clocks are power-hungry, expensive, and susceptible to electromagnetic interference at high sampling rates, which incur significant engineering expenses, particularly when considering deep submicron very-large-scale integration (VLSI) [7], [8], [9], [10], [11]. Therefore, asynchronous circuit systems and architectures that eliminate the need for a global clock have been proposed to achieve more energy-efficient designs, immunity to metastable behavior, and reduced electromagnetic interference [12], [13].

An integrate-and-fire time encoding machine (IF-TEM) is a widely-used asynchronous sampler due to its low power consumption [14] and simple hardware design [15]. In this mechanism, the non-negative input signal is first integrated and then compared to a threshold. The differences between successive time instances at which the threshold is reached are recorded, which ultimately leads to non-uniform time

The associate editor coordinating the review of this manuscript and approving it for publication was Jiawei Yang.

samples [16], [17], [18]. Time-based sampling hardware, which uses time instances (spikes) only for reconstruction, consumes less power than conventional uniform sampling-based hardware [8], [19], [20], [21], [22], [23], [24]. The ability to fully recover BL signals using TEM outputs has been extensively studied [1], [16], [18], [25], [26], [27], [28]. The results on time-encoding machines have also been extended to functions in shift-invariant spaces [29], typically by linking time encoding with a non-uniform sampling mechanism [30], [31]. More recent techniques exploit the signal's underlying structure, allowing accurate sampling and reconstruction at a sub-Nyquist rate [32], [33], [34], [35].

Several studies [9], [26], [31], [32], [34], [36] have investigated perfect reconstruction from IF-TEM samples but did not consider the impact of finite quantization. Lazar and Tóth [16] examined the effects of quantization for BL signals. They showed that the MSE upper bound for time quantization is exactly the same as the MSE upper bound for amplitude quantization when employing non-uniform sampling for the same number of bits. Our analysis, however, charts a different course. We compare the IF-TEM with quantization and the classical ADC that incorporates uniform sampling and quantization. These distinct lines of study can yield different outcomes, primarily due to the different systems being evaluated in relation to the IF-TEM sampler with quantization. Moreover, they did not explore the potential advantages that can be obtained by exploiting the interplay between the signal's energy, frequency, and maximal amplitude using an IF-TEM sampler with quantization in MSE terms, which is a focal point of our study.

The present work provides two primary advances. To begin, we analyze the quantization step size for the IF-TEM sampler, highlighting its distinctive characteristics when compared to standard sampling techniques. Specifically, by leveraging the interplay between the signal's energy, frequency, and maximal amplitude - where an increase in frequency or energy results in a corresponding increase in the signal's maximal amplitude and vice versa - we demonstrate that as the frequency of the IF-TEM input for BL signals or FRI models increases, the quantization step size decreases. This analysis sheds light on the unique behavior of the IF-TEM sampler in terms of quantization. Second, we demonstrate the superior performance of the IF-TEM sampler with quantization, achieving an average of 8 dB improvement compared to uniform classical samplers in terms of MSE for the scenarios considered, encompassing both BL and FRI signal models. In particular, we show that this improvement can be achieved by leveraging the interplay between the signal's characteristics and imposing specific conditions on IF-TEM parameter selection. Our results show the advantages of the IF-TEM sampler over traditional samplers, leading to reduced bit requirements for both the total number of samples and the number of bits per sample. Moreover, since the IF-TEM operates as a nonuniform, signal-dependent sampler, the theoretical insights developed in this work naturally extend to a broader class of time-based sampling schemes. As such, the proposed analysis provides a general framework for quantization and recovery in event-driven, signal-adaptive acquisition systems.

This manuscript is organized as follows: The research problem and essential background are presented in Section II. In Section III, we analyze the quantization strategies for BL signals using classical and IF-TEM sampling techniques. In Section IV, we present the derivation of recovery error bounds for BL signals resulting from quantization of IF-TEM time instance differences and compare it with classical sampler recovery error resulting from amplitude quantization. Additionally, we derive conditions under which the IF-TEM MSE upper bound is lower than the MSE of a classical sampler. The analysis of quantization approaches for both conventional and IF-TEM sampling methods with FRI signals is presented in Section V. Finally, we conclude the paper in Section VI.

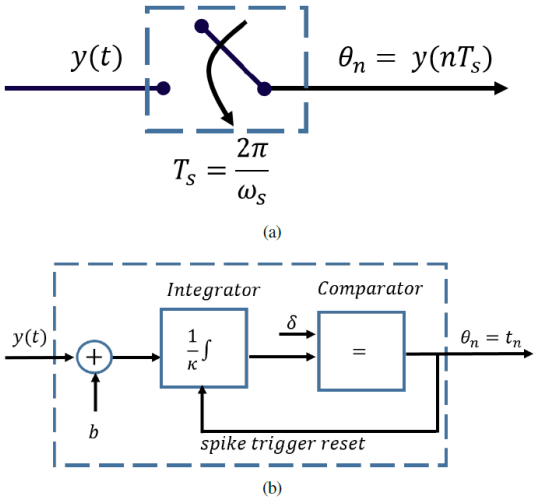

FIGURE 1. Schematic diagram of (a) classical sampler and (b) IF-TEM sampler, where b represents the bias, δ is the threshold, and κ is the IF-TEM integrator parameter.

II. PRELIMINARIES AND PROBLEM FORMULATION

Initially, we review key principles of the IF-TEM sampler and discuss signal characteristics. Subsequently, we outline our research objectives.

A. IF-TEM VERSUS TRADITIONAL SAMPLER

Conventional signal sampling involves uniform measurement of the signal's amplitude at specific time intervals. More specifically, given an input signal $x(t)$, the sampling process yields instantaneous samples $x(nT_s)$ with a sampling interval of T_s, as shown in Fig. 1a. In contrast, time encoding machines are a special type of sampling mechanism that encodes the input $x(t)$ by storing time instances instead of amplitudes.

An IF-TEM system is configured with three parameters: a bias value b, a scaling factor κ, and a threshold parameter δ, which is illustrated in Fig. 1b. The system processes a real-valued input signal $x(t)$, which is bounded by the condition $|x(t)| \leq c < b < \infty$. The encoding process begins by adding the bias b to the input signal and then scaling the resulting non-negative signal $x(t) + b$ by a factor of $1/\kappa$. This scaled signal undergoes integration, and when the integral reaches the threshold δ, the integrator resets, and we record the time differences between consecutive firing instants (see Fig. 2). From these consecutive firing instants, we calculate the time instances, which encode the input signal.

The IF-TEM input $x(t)$ and the time instances $\{t_n\}_{n\in\mathbb{Z}}$ are related by the equation:

$$\int_{t_n}^{t_{n+1}} x(\tau)\, d\tau = -b(t_{n+1} - t_n) + \kappa\delta. \tag{1}$$

The input signal's reconstruction utilizes measurements of form $\int_{t_n}^{t_{n+1}} x(\tau), d\tau$, which are derived from the firing times. According to (1) and given that $|x(t)|$ has an upper bound of c, we can establish bounds for the time interval $T_n = t_{n+1} - t_n$ as demonstrated in [16].

$$\Delta t_{\min} \triangleq \frac{\kappa\delta}{b+c} \leq T_n \leq \frac{\kappa\delta}{b-c} \triangleq \Delta t_{\max}. \tag{2}$$

Due to the bounded nature of temporal time differences, these values are the ones that are quantized and stored in memory. While this work focuses on quantization analysis under ideal conditions, practical IF-TEM implementations face additional challenges including timing jitter and circuit noise. These hardware aspects, along with circuit-level mitigation strategies, are addressed in detail [21].

B. SAMPLING AND RECONSTRUCTION OF BL SIGNALS

Signal reconstruction from IF-TEM measurements has been proven for inputs that are both c-bounded and 2Ω bandlimited within $\mathbf{L}^2(\mathbb{R})$ as shown in multiple works [1], [16], [18], [26].

Definition 1: A c-bounded and 2Ω bandlimited signal $x(t)$ is characterized by two properties: it satisfies the magnitude constraint $|x(t)| \leq c$ for some real number c, and its Fourier transform is non-zero only within the closed interval $[-\Omega, \Omega]$, where Ω represents frequency in radians per second.

The classical sampling theory, known as the Shannon-Nyquist theorem, establishes that complete reconstruction of a 2Ω bandlimited signal $x(t)$ is possible from its uniformly spaced samples $x(nT_s)$, provided the sampling frequency meets or exceeds the Nyquist rate of $\frac{\Omega}{\pi}$ Hz [5].

Definition 2: A signal $x(t) \in \mathbf{L}^2(\mathbb{R})$ is characterized as having finite energy $E \in \mathbb{R}$ if it satisfies

$$E = \int_{-\infty}^{\infty} |x(t)|^2 dt < \infty.$$

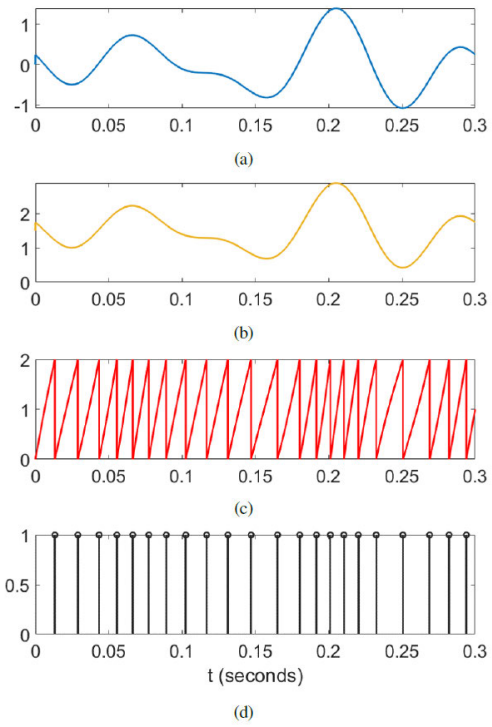

FIGURE 2. Sampling mechanism of a signal $x(t)$ using an IF-TEM sampler. (a) the signal $x(t)$. (b) the signal with an addition of a bias b such that $x(t) + b$ is a non negative signal. (c) the signal $x(t) + b$ is integrated and scaled, each time the threshold δ is reached the integrator resets and the time differences between consecutive time instances $T_n = t_n - t_{n-1}$ are recorded. (d) The IF-TEM series of time instances is calculated by summing up the time differences T_n starting from an initial time instant $t_0 = 0$.

An effective way to express the energy of a BL finite-energy function is by its Parseval's relation, which produces

$$E = \int_{-\infty}^{\infty} |x(t)|^2 dt = \frac{1}{2\pi} \int_{-\Omega}^{\Omega} |X(j\omega)|^2 d\omega, \tag{3}$$

where $X(j\omega)$ is the continuous-time Fourier transform of the signal $x(t)$. The relationship between bandwidth 2Ω and peak amplitude c can exist independently. When examining BL signals characterized by energy E, research by [37] establishes that Ω and c are connected through the expression:

$$c = \sqrt{\frac{E\Omega}{\pi}}. \tag{4}$$

Following the methodology outlined in [18], we implement an IF-TEM sampling system without a refractory period. The study in [18] and [31] demonstrates through iterative methods that complete reconstruction of BL signals is achievable using an IF-TEM configured with parameters b, κ, δ, provided that $b > c$ and:

$$\Delta t_{\max} = \frac{\kappa\delta}{b-c} < \frac{\pi}{\Omega}. \tag{5}$$

As demonstrated in (5), the bandwidth requirement exhibits inverse proportionality to the temporal gaps between firing instances. Specifically, successful reconstruction of the bandlimited input is achieved when the IF-TEM's firing

rate is above the Nyquist sampling rate. The process of signal recovery from IF-TEM data can be compared to reconstructing a BL signal using irregularly spaced amplitude measurements. The mathematical operator $\mathcal{R}$ that performs this reconstruction is expressed as:

$$\mathcal{R}(x(t)) = \sum_{i=1}^{\infty} \left(\int_{t_i}^{t_{i+1}} x(u)\mathrm{d}u \right) \mathrm{sinc}_{\Omega}(t - s_i), \tag{6}$$

where $s_i = \frac{t_i + t_{i+1}}{2}$ and

$$\mathrm{sinc}_{\Omega}(t) = \begin{cases} \dfrac{\sin(\Omega t)}{\pi t}, & \text{if } t \neq 0. \\ 1, & \text{otherwise.} \end{cases} \tag{7}$$

The values of $\int_{t_i}^{t_{i+1}} x(\tau)d\tau i \in \mathbb{Z}$ are evaluated from the IF-TEM output sequence $\{t_i\}_{i\in\mathbb{Z}}$ using (1). Assuming (5) holds, the $2\Omega c$-bounded BL signal $x(t)$ can be perfectly reconstructed using the following iterative algorithm, as showed in [16]:

$$x_{l+1}(t) = x_l(t) + \mathcal{R}\left(x(t) - x_l(t)\right), \tag{8}$$

where $l \in \mathbb{N}$ and $x_0(t) = \mathcal{R}(x(t))$. It is crucial to note that the signal $x(t)$ is known in analog form rather than digital form. Therefore, the subtraction $x - x_l$ can be generated using analog hardware and then passed through $\mathcal{R}$. In this case, $\lim_{l\to\infty} x_l(t) = x(t)$, and $\|x - x_l\| \leq r^{l+1}\|x\|$, where $r = \frac{\kappa\delta}{b-c}\frac{\Omega}{\pi} < 1$. Next, we discuss sampling and recovery for FRI signals.

C. SAMPLING AND RECONSTRUCTION OF FRI SIGNALS

Sampling and recovery of FRI signals, which have a limited number of degrees of freedom, are of great interest in applications such as radar and ultrasound [6], [38], [39]. FRI signals typically consist of shifted versions of a known pulse shape combined linearly. The processing pipeline for these signals incorporates three main components: specialized sampling kernels, an ADC, and parameter estimation. Through the sampling kernels, the FRI signal's information content spread out, enabling the parameter estimation stage to accurately determine timing delays and signal amplitudes while operating at reduced sampling frequencies with a finite number of samples (see Fig. 3). As shown in [34], the IF-TEM sampling approach can successfully reconstruct both periodic and aperiodic FRI signals. In this analysis, we specifically examine how to sample and reconstruct FRI signals that exhibit periodicity with period T.

A T-periodic FRI signal, denoted as $x(t)$, can be expressed mathematically as:

$$x(t) = \sum_{p\in\mathbb{Z}} \sum_{\ell=1}^{L} a_\ell h(t - \tau_\ell - pT), \tag{9}$$

In this representation, the FRI parameters consist of unknown pairs $\{(a_\ell, \tau_\ell) \,|\, \tau_\ell \in (0, T],\ a_\ell \in \mathbb{R}\}_{\ell=1}^{L}$, where a_ℓ represents the amplitudes and τ_ℓ represents the time delays. Both the pulse shape function $h(t) \in \mathbf{L}^2(\mathbb{R})$ and the number of pulses L are known quantities.

Given that $x(t)$ exhibits T-periodicity, it can be expressed using the following Fourier series expansion

$$x(t) = \sum_{k\in\mathbb{Z}} X[k]e^{jk\omega_0 t}, \tag{10}$$

where

$$X[k] = \frac{1}{T}H(k\omega_0)\sum_{\ell=1}^{L} a_\ell e^{-jk\omega_0\tau_\ell}, \tag{11}$$

and $\omega_0 = \frac{2\pi}{T}$. In this case, $H(\omega)$ represents the continuous-time Fourier transform of the pulse shape $h(t)$. For signal $x(t)$, the rate of innovation - defined as the number of degrees of freedom per unit time - equals $\frac{2L}{T}$.

Spectral analysis approaches, such as the annihilating filter (AF) method, can uniquely determine $a_\ell, \tau_\ell{}_{\ell=1}^{L}$ using a minimum of $2L$ Fourier series coefficients (FSCs) in classical systems and $2L + 2$ FSCs for IF-TEM configurations [6], [33], [34], [38]. As demonstrated in [6], these $2L$ FSCs $X[k]$ are sufficient to uniquely specify the FRI signal $x(t)$. The challenge of reconstructing the FRI signal can therefore be reformulated as accurately determining the necessary FSCs from the measured signal data. For IF-TEM systems, signal reconstruction has been analyzed specifically for c-bounded FRI inputs, with successful recovery possible when the IF-TEM parameters meet the following conditions [34]

$$\frac{1}{\Delta t_{\max}} \geq \frac{2L + 2}{T}. \tag{12}$$

This requirement parallels conventional FRI methodology, where exact reconstruction is guaranteed by sampling at a rate equal to the signal's innovation rate.

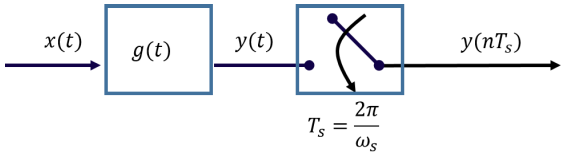

FIGURE 3. The FRI sampling system using kernel-based processing: The input FRI signal $x(t)$ undergoes filtering using a sampling kernel $g(t)$, followed by uniform instantaneous sampling below the Nyquist rate. The FRI signal parameters are then recovered from these sub-Nyquist measurements.

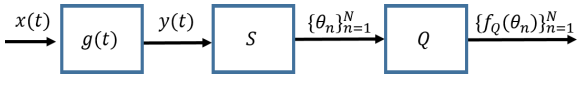

FIGURE 4. A quantized generalized sampling framework: The filtered signal $y(t) = (x * g)(t)$ is processed through a sampling operator S to produce discrete samples $\theta_n n \in I$ over a countable index set I. These samples then undergo quantization via operator Q to yield the quantized values $\{f_Q(\theta_n)\}_{n\in I}$.

D. PROBLEM FORMULATION

Previous studies have predominantly concentrated on perfect sampling and reconstruction using IF-TEM, disregarding the impact of quantization. The authors in [16] compared the reconstruction errors resulting from quantizing in the time and amplitude domains with non-uniform sampling framework. They showed that, with non-uniform sampling employed for amplitude quantization, the MSE upper bound for time quantization exactly matches that of amplitude quantization for the same number of bits. However, these investigations did not include a comparison between the IF-TEM sampler with quantization and the classical uniform sampler, nor did they explore the relationship between signal energy, frequency, and maximal amplitude. Additionally, the consideration of FRI signals was not part of their analysis. In contrast, our contribution addresses these gaps by conducting a comparison between the IF-TEM sampler with quantization and the classical uniform sampler, due to their widespread use in practical systems. Additionally, we examine the interplay between signal energy, frequency, and maximal amplitude to shed light on its impact on the quantization step size for both the IF-TEM and the classical sampler.

Our objective is to capitalize on this relationship and analyze the performance in terms of MSE. Specifically, we aim to evaluate and compare the signal recovery error for both the IF-TEM and classical setups when reconstructing a signal $x(t)$ from its quantized samples, addressing both FRI and BL signal categories. For the BL case, the analysis encompasses signals that are 2Ω bandlimited and c-bounded in $\mathbf{L}^2(\mathbb{R})$, with energy constrained by $E < \infty$. For FRI signals, we concentrate on T-periodic expressions as shown in (9), aiming to determine the characteristic parameters $a_\ell, \tau_\ell{}_{\ell=1}^{L}$ through quantized IF-TEM measurements, where Fourier series coefficients are computed from the quantized data.

Figure 4 demonstrates a comprehensive sampling framework incorporating quantization. In this system, the initial signal $x(t)$ undergoes processing through a sampling kernel $g(t)$ to produce $y(t)$. We then extract a series of measurements $\theta_{n n\in I}$ from $y(t)$, where I represents a countable index set. The operations of sampling and quantization are denoted by S and Q respectively. Two distinct sampling approaches are possible: a standard sampling method shown in Fig. 1(a) where $\theta_n = y(nT_s)$, or an IF-TEM configuration illustrated in Fig. 1(b) where $\theta_n = t_n$.

In the case of BL signals, the sampling kernel can either be implemented as a low-pass filter or omitted entirely. When processing FRI signals, regardless of whether using IF-TEM or traditional methods, the kernel $g(t)$ is engineered to enable calculation of $2L+2$ FSCs of $x(t)$ from the measurement set $\theta_{n n\in I}$, with $|I| \geq 2L+2$. The FSCs can be extracted from these measurements through a SoS filter, as demonstrated in [34] and [39].

The measurements θ_n obtained from $x(t)$ undergo quantization following the sampling process. Traditional ADC systems employ uniform quantization for the amplitude samples $y(nT_s)$. In the IF-TEM framework, uniform quantization is applied to the temporal intervals between encodings, $T_n = t_{n+1} - t_n$, yielding quantized intervals denoted as $\hat{T}_n$

The subsequent analysis first explores quantization approaches for both traditional and IF-TEM sampling methods when applied to BL signals, including guidelines for optimal quantization step size selection. We then evaluate the reconstruction quality by developing MSE upper bounds for BL signal recovery using quantized measurements $f_Q(\theta_n)$ in both frameworks. Our investigation reveals the optimal IF-TEM parameter configurations that achieve enhanced MSE performance relative to classical sampling, while maintaining consistent quantization resolution. The analysis concludes by extending these performance advantages to FRI signal scenarios, demonstrating consistently superior MSE outcomes compared to conventional sampling methods.

III. QUANTIZATION ANALYSIS

This section examines the quantization approaches employed in both traditional and IF-TEM sampling frameworks when dealing with BL signals.

A. CLASSICAL AND IF-TEM SAMPLERS QUANTIZATION STEP

We first demonstrate that as in IF-TEM the energy E or the frequency of the BL signal grows, the dynamic range $\Delta t_{max} - \Delta t_{min} = \frac{\kappa\delta}{b-c} - \frac{\kappa\delta}{b+c}$ of each time sample decreases. We demonstrate that unlike the conventional approach, for a specific selection of IF-TEM parameters and fixing the ratio between b and c, increasing the frequency or energy of the signal increases the quantizer's resolution [1].

$$|x(t)| \leq c \triangleq \sqrt{\frac{E\Omega}{\pi}}. \tag{13}$$

The c-bounded nature of $x(t)$ ensures that all instantaneous measurements $x(nT_s)$ fall within the interval $[-c, c]$. The quantization process uses N bits to generate $K = 2^N$ equally spaced levels. The classical sampler quantization step size is given by

$$\Delta_{\text{classic}} = \frac{2c}{K}. \tag{14}$$

It is worth noting that when quantizing the amplitude differences, akin to quantizing the time differences in IF-TEM, the range of the instantaneous samples $x((n+1)T_s) - x(nT_s)$ lies within the interval $[-2c, 2c]$. In this scenario, the quantization step size for the amplitude differences in the classical sampler can be expressed as:

$$\Delta_{\text{classic diff}} = \frac{4c}{K} = 2\Delta_{\text{classic}}. \tag{15}$$

Consequently, by utilizing the same number of bits $N = \log_2 K$, the quantization step resolution for the amplitude differences method is inferior to that of the classical method, where only the amplitudes themselves are quantized. Therefore, throughout this work, the classical ADC baseline always refers to direct amplitude quantization with step size 14. The difference-quantization case in (15) is not used for performance comparisons and is included here to explain why we quantize the amplitudes directly rather than their differences. To analyze this further, we examine how the IF-TEM quantization strategy performs relative to conventional quantization methods.

For the IF-TEM approach, quantization is applied to the time differences T_n. According to (2), these time differences span the interval $[\frac{\kappa\delta}{b+c}, \frac{\kappa\delta}{b-c}]$. When employing uniform quantization with K levels, the resulting IF-TEM quantization step can be expressed as

$$\Delta_{\text{IF-TEM}} = \frac{\frac{\kappa\delta}{b-c} - \frac{\kappa\delta}{b+c}}{K} = \frac{\kappa\delta}{(b+c)(b-c)}\frac{2c}{K}. \tag{16}$$

The integrator parameter κ is determined by the circuit design and typically remains constant [21], [26]. The comparator threshold δ and bias b offer more flexibility for adjustment. To satisfy the sampling density requirement in (5), one can either enhance the bias b or reduce the threshold δ. Since DC voltage sources generate both b and δ, larger parameter values demand increased power input. For power efficiency, these values should be minimized. Yet with fixed b and κ, reducing δ produces firing rates exceeding the minimum desirable firing rate. A balanced solution involves keeping δ and κ constant while choosing the bias to satisfy $b > c$ where $b = \alpha c$, with $\alpha > 1$ and $b - c = \epsilon > 0$. To examine the relationship between signal frequency Ω and $\Delta_{\text{IF-TEM}}$, we maintain constant δ and κ while allowing b to vary.

The following analysis demonstrates that the quantization step size $\Delta_{\text{IF-TEM}}$ exhibits an inverse relationship with increasing signal frequency Ω. The following theorem formalizes this relationship.

Theorem 1: Consider an IF-TEM sampler, followed by a K-level uniform quantizer, where $K = 2^N$ and N denotes the number of bits. For 2Ω-BL signals with maximal energy E, given a fixed $\alpha > 1$, let the IF-TEM bias be represented by b, such that $b = \alpha c$, where c is defined in (13). Under Nyquist-like constraint (5), the quantization step $\Delta_{\text{IF-TEM}}$ decreases as the energy E or the frequency Ω increases.

Proof: Fix κ and δ. The bias is chosen such that $b = \alpha c$ with fixed $\alpha > 1$. Substituting b into (16), we have

$$\Delta_{\text{IF-TEM}} = \frac{\kappa\delta}{(\alpha+1)(\alpha-1)}\frac{2}{cK}. \tag{17}$$

Using condition (13) and (5) results in

$$\Delta_{\text{IF-TEM}} = \frac{\kappa\delta}{(\alpha+1)(\alpha-1)}\frac{2}{K}\sqrt{\frac{\pi}{E\Omega}}. \tag{18}$$

Thus, with an increasing signal's energy E or frequency Ω, the IF-TEM quantization step size decreases. □

Note that Theorem 1 highlights a significant difference from the classical method: increasing the signal's frequency or energy, which correlates with the maximal amplitude c, leads to an improved resolution of the quantizer. While the preceding analysis shows that increased signal energy or frequency reduces the IF-TEM's quantization step size, this alone does not guarantee a corresponding improvement in reconstruction error. Although smaller quantization steps are generally conducive to more accurate recovery, their impact must be interpreted within a broader theoretical framework. In particular, the sampling and reconstruction scheme plays a critical role in shaping how quantization errors propagate through the system.

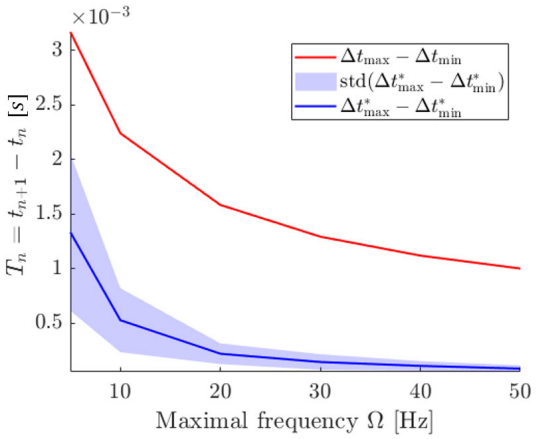

FIGURE 5. Time instances differences in IF-TEM for BL signals as a function of the frequency band. In red: the difference $\Delta t_{\max} - \Delta t_{\min}$, as defined in (2). In blue: the solid line shows the average values of $\Delta t^*_{\max} - \Delta t^*_{\min}$, which are the real difference. See the range in Table 1.

TABLE 1. Time instants range (in seconds) for the IF-TEM with BL signals.

Frequency [HZ]	5	10	30	50
$\Delta t_{\max} - \Delta t_{\min}[e{-}04]$	32	22	13	10
$\Delta t^*_{\max} - \Delta t^*_{\min}[e{-}04]$	13	5.2	1.4	0.85
$\Delta t_{\max} - \Delta t_{\min}$[decimal]	0.0032	0.0022	0.0013	0.0010
$\Delta t^*_{\max} - \Delta t^*_{\min}$[decimal]	0.0013	0.00052	0.00014	0.000085

To underscore the significance of this relationship, consider an example with a non-fixed $\alpha > 1$, where $b = \alpha c$. Given a fixed K (corresponding to a fixed number of bits per sample, using uniform quantizer) and choosing $\kappa = \delta = b = 1$: In the first case: For $c = \frac{1}{4}$, this corresponds to $\alpha = 4$, resulting in $\Delta_{\text{IF-TEM}} = \frac{8}{15K}$. In the second case: For $c = \frac{1}{2} > \frac{1}{4}$ (indicating an increase in c), this relates to $\alpha = 2$, yielding $\Delta_{\text{IF-TEM}} = \frac{4}{3K}$. Despite the increase in c, we observe an increase in the quantization step size. This example clearly demonstrates that if α is not fixed, simply increasing the signal amplitude c does not guarantee a reduction in quantization step size, which is why

our theoretical analysis requires maintaining a constant ratio $\alpha = \frac{b}{c} > 1$ to achieve the desired inverse relationship between signal characteristics and quantization performance. The relation between the amplitude c and the bias b needs to obey the Nyquist condition given in (5). Moving forward, we assume that the relationship between b and c is defined as $b = \alpha c$, with a constant $\alpha > 1$.

An analysis of (14), (15), and (17) reveals contrasting behaviors: while classical sampling exhibits larger quantization steps as the bandlimited signal amplitude increases, IF-TEM demonstrates the opposite trend with decreasing step sizes at higher amplitudes. Moreover, as $\Omega > 0$ increases, the sampling instants become more densely packed, resulting in smaller T_n values and a narrowing gap between $\Delta t_{\min}$ and $\Delta t_{\max}$ (see Fig. 5 and Table 1). Thus, as shown in Section IV, this characteristic leads to reduced quantization error, allowing IF-TEM to achieve superior quantization performance compared to classical methods when using the same number of bits.

As a final remark, for fixed K, a higher energy E or frequency Ω of the BL signal leads to an increased number of samples N across both IF-TEM and conventional approaches. As a result, both methods experience a growth in their total bit count. To conduct a fair analysis, we maintain identical sample numbers between the conventional and IF-TEM techniques.

B. EVALUATION RESULTS

We now present empirical evidence showing that, with a fixed number of quantization bits, the quantization step size decreases when either the bandwidth or frequency of the BL signal increases.

We analyze a BL signal $x(t)$ with bandwidth 2Ω. The amplitude of the signal is constrained by $|x(t)| \leq c$, where c, defined as $c = \sqrt{(E\Omega)/\pi}$. In our experimental setup, we set $E = 1$ and investigate the reconstruction performance of the IF-TEM system after quantization over a frequency range, with Ω varying between 5 and 50 Hz. The input signal is represented by

$$x(t) = \sum_{n=-i}^{i} a[n] \operatorname{sinc}\left(\frac{t - nT_s}{T_s}\right), \tag{19}$$

where $i = 3$, $T_s = \frac{1}{2\Omega}$, and $a[n]$ are 100 uniform i.i.d sets within the range $[-1, 1]$. Subsequently, the signal is normalized to have an energy of $E = 1$.

For the IF-TEM implementation, we configure the system with constant parameters $\delta = 0.075$ and $\kappa = 0.4$. To ensure an adequate number of samples for accurate reconstruction, the bias b is set to four times the amplitude bound c (expressed as $b = 4c$, yielding $\alpha = 4$, and satisfies the condition $|x(t)| \leq c$. The uniform quantizer used has $N = 12$ bits. The system configuration uses specific IF-TEM parameters: a fixed value of $\delta = 0.075$ and $\kappa = 0.4$. For reliable signal reconstruction, we set the bias parameter to $b = 4c$, i.e, $\alpha = 4$, and satisfies the condition $|x(t)| \leq c$. The uniform quantizer used has $N = 12$ bits. We define $\Delta t^*_{\max}$ and $\Delta t^*_{\min}$ as empirical bounds computed from the actual maximum and minimum time intervals observed in simulations. We show that as the signal frequency increases, the time instance differences and their range $\Delta t_{\min} - \Delta t_{\max}$ become smaller. The findings are presented in Fig. 5 and Table 1.

Since the IF-TEM parameters, κ and δ are chosen to be constant, and $b = 4c$, from (2) and (4), it is evident that only the maximal amplitude $c = \sqrt{(E\Omega)/\pi}$, or the frequency Ω, affects the interval $\Delta t_{\max} - \Delta t_{\min}$ (see Fig. 5). In order to examine the frequency influence not only on the boundaries but also on the signal itself, based on the fact that $|x(t)| \leq c$, we define tighter bounds on the difference between the time instances as follows:

$$\Delta t^*_{\max} = \frac{\kappa\delta}{b - \max(x(t))} \leq \frac{\kappa\delta}{b - c} = \Delta t_{\max}, \tag{20}$$

and

$$\Delta t^*_{\min} = \frac{\kappa\delta}{b + \max(x(t))} \geq \frac{\kappa\delta}{b + c} = \Delta t_{\min}. \tag{21}$$

Note that $\Delta t^*_{\max} - \Delta t^*_{\min} \leq \Delta t_{\max} - \Delta t_{\min}$. This relationship enables enhanced quantization efficiency at higher frequencies: despite maintaining a fixed 12-bit quantizer resolution, we achieve improved precision for higher-frequency bandlimited signals due to the compressed temporal sampling intervals.

Since a reduced quantization step size does not by itself ensure improved reconstruction accuracy, its effect must be understood in the context of the sampling and reconstruction scheme. The following section establishes the conditions under which, together with the IF-TEM architecture, a smaller quantization step size yields superior MSE performance relative to classical ADC sampling.

IV. RECONSTRUCTION ERROR WITH QUANTIZATION

Next, utilizing Theorem 1, which shows that the quantization error $\Delta_{\text{IF-TEM}}$ decreases with increasing amplitude c or frequency Ω of the BL signal, we demonstrate that the IF-TEM method achieves a lower MSE compared to the conventional ADC approach.

A. IF-TEM QUANTIZATION NOISE

In this section, we introduce an upper bound for the error resulting from time sequence quantization. Lazar and Tóth [16] established an upper bound for the reconstruction error associated with the asynchronous sigma-delta modulator (ASDM) sampler. They demonstrated that the MSE upper bound for time quantization is equal to that of amplitude quantization under non-uniform sampling, assuming a fixed number of bits. We use the same MSE metric as in [16] to evaluate the reconstruction error of the IF-TEM. Our work, however, offers a distinct perspective. We evaluate the MSE of the IF-TEM with quantization, and compare it with the conventional ADC that employs uniform sampling and quantization under the same number of bits and samples.

Given the distinctions in our methodological approaches, it is expected that our results may differ, particularly when considering the specific characteristics of the IF-TEM sampler with quantization we introduce here. Note that Lazar and Tóth [16] did not explore the relationship between a signal's energy, frequency, and maximal amplitude in the context of the time-based sampler MSE. Yet, even if this aspect had been investigated, their conclusions, anchored in non-uniform sampling for both ASDM and traditional samplers, would remain the same. In contrast, we show that the quantization step size of the IF-TEM sampler, together with its configuration (e.g., the bias-to-amplitude ratio α), can be decreased when the energy or maximal frequency of a BL signal is increased or the number of pulses of an FRI signal is increased. Consequently, under specific parameter configurations, the IF-TEM sampler exhibits a strictly lower MSE bound compared to a classical ADC with equivalent number of samples and bit depth.

In the following, we introduce an upper bound for the IF-TEM MSE, as described in Theorem 2 building upon the relationships between the signal's energy, frequency, and maximal amplitude (4), as well as the connection between the signal's maximal amplitude c and the IF-TEM bias b, that is, $b = \alpha c$ with a constant $\alpha > 1$. Drawing on Theorem 1, we can explain this behavior through the inverse relationship between the quantization step size $\Delta_{\text{IF-TEM}}$ and both the maximal signal's amplitude c and frequency Ω. When comparing performance metrics, our findings indicate that the IF-TEM sampling approach outperforms traditional sampling methods in terms of MSE), while maintaining an equivalent number of bits and measurements.

Consider the scenario where the sequence of time instances $\{t_i\}_{i\in\mathbb{Z}}$ is subject to measurement with limited precision. Denote the recovered values by $\{\hat{t}_i\}_{i\in\mathbb{Z}}$. We define $T_i = t_{i+1} - t_i$ and $\hat{T}_i = \hat{t}_{i+1} - \hat{t}_i$ for all $i \in \mathbb{Z}$. Assume that $\hat{\mathcal{R}}$ is a reconstruction operator defined by (see (6)):

$$\hat{\mathcal{R}}(x(t)) = \sum_{i=1}^{\infty} \left(\int_{\hat{t}_i}^{\hat{t}_{i+1}} x(u)\mathrm{d}u \right) \operatorname{sinc}_{\Omega}(t - \hat{s}_i), \tag{22}$$

where $\hat{s}_i = \dfrac{\hat{t}_{i+1} + \hat{t}_i}{2}$ and $\operatorname{sinc}_{\Omega}(t)$ is defined in (7). In this case, it was shown in [16] that the following expressions hold:

$$x(t) = \sum_{k\in\mathbb{N}} (I - \hat{\mathcal{R}})^k \hat{\mathcal{R}} x(t), \tag{23}$$

and

$$\hat{x}(t) = \sum_{i\in\mathbb{N}} (I - \hat{\mathcal{R}})^i \sum_{l\in Z} [\kappa\delta - b\hat{T}_l] \operatorname{sinc}_{\Omega}(t - \hat{s}_l)). \tag{24}$$

The reconstruction algorithm produces the error signal $e(t) = x(t) - \hat{x}(t)$, where $\hat{x}(t))$ denotes the reconstructed signal. Using (23) and (24), we can express the error as a summation:

$$e(t) = \sum_{k\in Z} (I - \hat{\mathcal{R}})^k \sum_{l\in Z} \epsilon_l \operatorname{sinc}_{\Omega}(t - \hat{s}_l), \tag{25}$$

where

$$\epsilon_l = [\kappa\delta - b\hat{T}_l] - \int_{\hat{t}_l}^{\hat{t}_{l+1}} x(u)\mathrm{d}u. \tag{26}$$

When there is no quantization error, we have $\hat{t}_l = t_l$. Substituting this into (26), and using (1) leads to $\epsilon_l = 0$ and $e(t) = 0$. However, with quantization, $\hat{t}_l$ may not necessarily be equal to t_l and $\hat{T}_l$ may not necessarily be equal to T_l, rendering (1) inapplicable, and thus ϵ_l may not be zero.

Considering the definition of (26), we observe that since $x(t)$ is BL, $\int_{\hat{t}_l}^{\hat{t}_{l+1}} x(u)\mathrm{d}u \in \ell^2$, while $[\kappa\delta - b\hat{T}_l]$ may not belong to ℓ^2 due to the quantization of the time differences. In the absence of quantization, $[\kappa\delta - bT_l] = \int_{t_l}^{t_{l+1}} x(u)\mathrm{d}u \in \ell^2$. Consequently, $e(t)$ as defined in (25) may not necessarily be in $L^2(\mathbb{R})$ since it is a series of shifted sinc functions with coefficients that may not be in ℓ^2. Hence, computing the MSE by employing an L_2 norm on (25) is not a straightforward task. Instead, we follow [16] and define a squared error measure ε^2 of the quantization process as follows

$$\varepsilon^2 = \lim_{n\to\infty} \frac{1}{2n\Delta t_{\min}} ||e\mathbb{1}_{[-n\Delta t_{\min}, n\Delta t_{\min}]}||^2, \tag{27}$$

where e is the error signal given by (25), $\mathbb{1}_{[-n\Delta t_{\min}, n\Delta t_{\min}]}$ is an indicator function, $\Delta t_{\min}$ is the minimum width between any two consecutive time instants, T_k is the time difference between the k-th and $(k+1)$-th time instants, and

$$||e\mathbb{1}_{[-n\Delta t_{\min}, n\Delta t_{\min}]}||^2 = \int_{\mathbf{R}} e^2(t)\mathbb{1}_{[-n\Delta t_{\min}, n\Delta t_{\min}]}(t)dt. \tag{28}$$

If the error in quantizing the time differences is modeled as a random process, ϵ_l becomes a random quantity. Consequently, ε^2 and $e(t)$ are also random. Therefore, we focus on the expectation, $\mathbb{E}[\varepsilon^2]$, which we will refer to as the MSE. In the following theorem, we introduce an upper bound for the MSE of the IF-TEM $\mathbb{E}[\varepsilon^2]$ when the quantization error on the recorded time differences is modeled as a uniformly distributed i.i.d. sequence. **Remark:** Theorem 2 assumes ideal quantization with i.i.d. uniform errors, neglecting circuit non-idealities such as comparator jitter and integrator leakage. These assumptions enable tractable analytical bounds; practical deviations are characterized experimentally in [21].

Theorem 2: Let $x(t)$, $t \in \mathbb{R}$ be a signal BL to $[-\Omega, \Omega]$. Consider an IF-TEM sampler followed by a K-level uniform quantizer with $N = \log_2 K$ bits. Let E be the maximal energy of $x(t)$, and let the relationship between E, Ω and c be given by $c = \sqrt{E\Omega/\pi}$. Let $b = \alpha c$ for any fixed $\alpha > 1$, where b represents the IF-TEM bias. Consider a sequence of uniform i.i.d random variables $d_k = \hat{T}_k - T_k$ on $[-\frac{\Delta_{\text{IF-TEM}}}{2}, \frac{\Delta_{\text{IF-TEM}}}{2}]$ as the quantization error, where $\Delta_{\text{IF-TEM}}$ defined in (17). Then, the MSE is upper bounded by

$$\mathbb{E}[\varepsilon^2] < \frac{R}{(1-R)^2} \left(\frac{\alpha+1}{\alpha-1}\right) \left(\frac{E\Omega}{3\pi}\right) \frac{1}{2^{2N}}, \tag{29}$$

where $R = \left(\dfrac{\kappa\delta}{\alpha-1}\right)\sqrt{\frac{\Omega}{E\pi}} < 1$.

Proof: Consider a BL signal $x(t)$ with $t \in \mathbb{R}$, confined to the frequency range $[-\Omega, \Omega]$. The maximal amplitude of this signal is represented by c. The signal processing system consists of an IF-TEM sampler cascaded with a uniform quantizer that employs K levels, utilizing $N = \log_2 K$ bits. Initially, we focus on proving Lemma 1, for which the proof can be found on Appendix A. In this scenario, the relation $b = \alpha c$ with a fixed $\alpha > 1$, and the relationship between E, Ω, and c which is given by $c = \sqrt{E\Omega/\pi}$, is not considered. The quantization step size in this case follows from (16). The parameters of the IF-TEM, $\{\kappa, b > c, \delta\}$, are solely selected to adhere to the Nyquist criterion (5), that is, $r = \frac{\kappa\delta\Omega}{\pi(b-c)} < 1$.

Lemma 1: Suppose $d_k = \hat{T}_k - T_k \sim \text{Unif}(-\frac{\Delta_{\text{IF-TEM}}}{2}, \frac{\Delta_{\text{IF-TEM}}}{2})$ is the quantization error, where $\Delta_{\text{IF-TEM}}$ defined in (16). The MSE $\mathbb{E}[\varepsilon^2]$, which ε^2 given in (27), can be upper bounded as

$$\mathbb{E}[\varepsilon^2] < \frac{b+c}{T\kappa\delta}\left(\frac{b+c}{1-r}\right)^2 \frac{\Delta^2_{\text{IF-TEM}}}{12}, \tag{30}$$

where the Nyquist interval $T = \frac{1}{f_{nyq}} = \frac{\pi}{\Omega}$. Our derivation of Lemma 1 is an independent contribution that addresses a key limitation in [16]. While the structure of the Lemma is similar, our proof (see Appendix A) rigorously analyzes the error dynamics induced by cumulative quantization in IF-TEM systems. Specifically, we establish boundedness and convergence under uniformly distributed i.i.d. quantization noise.

When considering a fixed ratio between b and c given by $\alpha = \frac{b}{c} > 1$, the IF-TEM quantization step size from Theorem 1 is valid and defined as $\Delta_{\text{IF-TEM}} = \frac{\kappa\delta}{(\alpha+1)(\alpha-1)}\frac{2}{cK}$. Incorporating this step size and the bound from Lemma 1, and considering the relationship between E, Ω, and c described earlier (4), we deduce the following upper bound

$$\mathbb{E}[\varepsilon^2] < \frac{R}{(1-R)^2}\left(\frac{\alpha+1}{\alpha-1}\right)\left(\frac{E\Omega}{3\pi}\right)\frac{1}{2^{2N}}, \tag{31}$$

where $R = \left(\frac{\kappa\delta}{\alpha-1}\right)\sqrt{\frac{\Omega}{E\pi}} < 1$. Here, $R < 1$ since the IF-TEM parameters $\{\kappa, b, \delta\}$ are chosen to satisfy the Nyquist criterion (5), and achieve perfect recovery of the BL signal $x(t)$ from the IF-TEM time instances. This completes our proof. □

Remark 1: A related bound for Lemma 1 appears in [16], however, their derivation does not account for the propagation of quantization errors, which leads to a linearly growing variance in the recovered time instances. Our analysis addresses this issue explicitly by bounding the deviation (see Appendix A).

To demonstrate the applicability of Theorem 2, we present in Fig. 6 the relationship between the empirical MSE in decibels and the energy and frequency of a signal. For the simulations in Fig. 6, reconstruction from the quantized IF-TEM spike intervals was carried out using the matrix pseudoinverse method of [16]. The number of IF-TEM samples determines the reconstruction matrix size, while the quantization bit depth fixes the resolution. In contrast to the classical scheme, where with fixed N bits the quantization step increases with bandwidth, in IF-TEM the relation $\sqrt{\frac{E\Omega}{\pi}}$ ensures that the quantization step decreases as frequency or energy increase. Consequently, Fig. 6 demonstrates that with fixed α and bit budget, the MSE decreases with frequency and energy, highlighting the fundamental advantage of the IF-TEM approach. Note that as the energy and frequency of the signal increase, so does the total number of time instances t_n, which in turn results in a larger oversampling factor. Therefore, we select the IF-TEM sampler parameters such that a low oversampling factor is achieved while maintaining a good reconstruction in terms of MSE. The oversampling factor is defined as the ratio between the actual IF-TEM sampling rate and the Nyquist rate for a given bandwidth.

Prior work [34] established that an IF-TEM's firing rate F_R, when operating with parameters b, κ, and δ, is bounded from both above and below by

$$\frac{1}{\Delta t_{\max}} = \frac{b-c}{\kappa\delta} \le F_R \le \frac{b+c}{\kappa\delta} = \frac{1}{\Delta t_{\min}}. \tag{32}$$

Note that for a BL signal $x(t)$, $t \in \mathbb{R}$ defined over $[-\Omega, \Omega]$, the firing rate can be expressed as

$$F_R = OS \cdot f_{nyq}, \tag{33}$$

where OS is the oversampling factor and $f_{nyq} = \frac{\Omega}{\pi}$ is the Nyquist rate. Consequently, we have the relationship

$$f_{nyq}\Delta t_{\min} \le \frac{1}{OS} \le f_{nyq}\Delta t_{\max}. \tag{34}$$

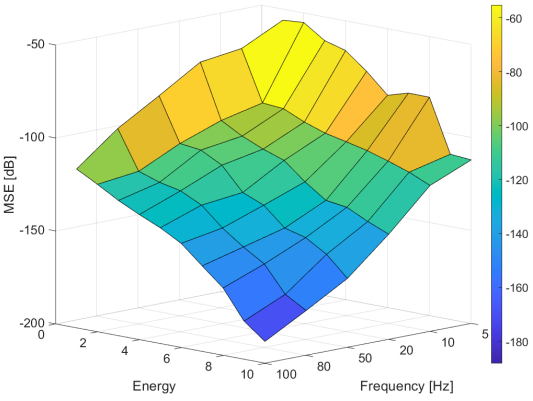

FIGURE 6. Empirical MSE results using the IF-TEM sampler as a function of signal frequency and energy with 12-bit quantization. Increasing frequency or energy leads to decreased MSE.

Fig. 7 displays the frequency and energy dependence of the oversampling factor. As the frequency and energy of the signal increase, its maximal amplitude c also increases, resulting in an increase in the oversampling ratio. Within each experimental configuration, α is kept constant, so the oversampling factor varies naturally according to equation (33). With κ and δ fixed, the bias b is set proportionally to the signal's maximum amplitude c through $b = \alpha c$ with $\alpha > 1$.

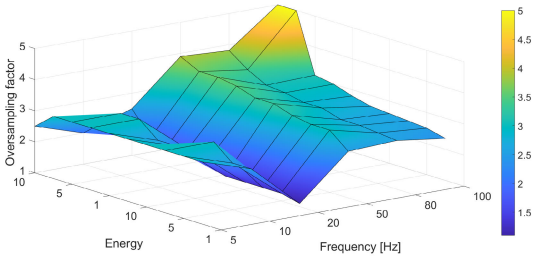

FIGURE 7. Oversampling factor as a function of energy and frequency. To fairly compare the MSE of the approaches in our simulations, we use the same amount of bits and a moderate oversampling factor.

In practice, we observed oversampling factors up to 6; this value represents the maximal OS obtained in our simulations and serves as an upper bound chosen for computational feasibility and to enable fair comparison with classical ADC. These findings suggest that careful selection of the IF-TEM sampler parameters can achieve a low oversampling ratio while maintaining good signal reconstruction accuracy in terms of MSE.

B. COMPARISON WITH CLASSICAL METHOD

We next compare the performance of conventional and IF-TEM reconstruction techniques in terms of their MSE. Our goal is to evaluate the advantages of using IF-TEM sampler over conventional sampling in the presence of quantization.

Consider a uniform quantizer with $K = 2^N$ levels and N quantization bits. The quantization step size is determined using (14), which yields

$$\Delta_{\text{classic}} = \frac{2c}{K}.$$

Here, c denotes the maximal amplitude of the signal, and K represents the total number of quantization levels. Assuming that the quantization error is a sequence of uniform i.i.d random variables on $[-\Delta_{\text{classic}}/2, \Delta_{\text{classic}}/2]$, the quantization error for the classical uniform sampler for the BL signal becomes [40]

$$\text{MSE}_{\text{classic}} = \frac{\Delta^2_{\text{classic}}}{12} = \frac{(2c/K)^2}{12} = \frac{c^2}{3K^2}, \tag{35}$$

where $\text{MSE}_{\text{classic}}$ denotes the quantization error. When oversampling the signal, the quantization error becomes [40]

$$\text{MSE}_{\text{classic}} = \frac{\Delta^2_{\text{classic}}}{12} \cdot \frac{1}{OS} = \frac{c^2}{3K^2} \cdot \frac{1}{OS}. \tag{36}$$

We use (36) to compute the quantization error for the classical ADC when oversampling is present, with oversampling factors up to 6 in our comparisons.

In practical scenarios, both the classical sampler and the IF-TEM sampler operate over a finite time interval, resulting in a finite number of samples. To evaluate their performance, we calculate the MSE of the IF-TEM sampler over a sufficiently large time window, which closely approximates the expression in (27). The calculated MSE of the IF-TEM sampler over this large time window is bounded by the upper bounds derived in Theorem 2. The approximation using a sufficiently large time window enables a direct comparison of the quantization error metrics between classical ADC and IF-TEM sampler. Our aim is to compare the Nyquist ADC quantization error given by (36), which has quantization step size $\Delta_{\text{classic}} = \frac{2c}{K}$ as defined in (14), to the IF-TEM MSE upper bound given in (29). We summarize our findings in the theorem below.

Theorem 3: Consider a signal $x(t)$, $t \in \mathbb{R}$ which is BL to $[-\Omega, \Omega]$. The signal $x(t)$ is sampled by an IF-TEM sampler and a classical uniform sampler with a fixed oversampling OS. Both the samplers are followed by a K-level uniform quantizer with $N = \log_2 K$ bits. Let E be the maximal energy of $x(t)$, and let the relationship between E, Ω and c be given by $c = \sqrt{E\Omega/\pi}$. Let $b = \alpha c$ for any fixed $\alpha > 1$, where b represents the IF-TEM bias. A sufficient condition for IF-TEM to exhibit lower quantization noise than Nyquist ADC for a fixed number of bits N is given by

$$\left(\frac{1}{2(1-R)^2}\right)\left(\frac{\alpha+1}{\alpha-1}\right)^2 \leq 1, \tag{37}$$

where $\alpha = \frac{b}{c} > 1$, and $R = \left(\frac{\kappa\delta}{\alpha-1}\right)\sqrt{\frac{\Omega}{E\pi}} < 1$.

Proof: Using (29), (34), (36), (4) and $b = \alpha c$, where $\alpha > 1$, it follows that

$$\begin{aligned}
\mathbb{E}[\varepsilon^2] &< \frac{R}{(1-R)^2}\left(\frac{\alpha+1}{\alpha-1}\right)\left(\frac{E\Omega}{3\pi}\right)\frac{1}{2^{2N}} \\
&= \left(\frac{E\Omega}{3\pi}\right)\frac{1}{2^{2N}}\frac{1}{(1-R)^2}\left(\frac{\alpha+1}{\alpha-1}\right)\left(\frac{\kappa\delta}{\alpha-1}\right)\sqrt{\frac{\Omega}{E\pi}} \\
&= \left(\frac{E\Omega}{3\pi 2^{2N}}\right)\frac{1}{(1-R)^2}\left(\frac{\alpha+1}{\alpha-1}\right)^2\left(\frac{\kappa\delta\Omega}{\pi c(\alpha+1)}\right) \\
&= \left(\frac{E\Omega}{3\pi 2^{2N}}\right)\frac{1}{(1-R)^2}\left(\frac{\alpha+1}{\alpha-1}\right)^2\left(\frac{F_{Nyq}}{2}\Delta t_{\min}\right) \\
&\leq \frac{1}{2}\cdot\underbrace{\frac{c^2}{3K^2}\frac{1}{OS}}_{\text{MSE}_{\text{classic}}}\cdot\frac{1}{(1-R)^2}\left(\frac{\alpha+1}{\alpha-1}\right)^2
\end{aligned} \tag{38}$$

To ensure that the IF-TEM has lower quantization noise than the Nyquist ADC, (37) serves as a sufficient condition.□

In the simulations shown in Figures 5–7, we follow the same parameter setting used in the theoretical analysis: κ and δ are fixed, and the bias b is varied proportionally with the signal's maximum amplitude c, using $\alpha > 1$ fixed. This reflects the practical flexibility of tuning b, as comparator thresholds δ typically support only a limited set of discrete values in hardware. These experiments empirically validate the predictions of Theorems 1 and 3.

In contrast, in the experiments shown in Figures 8–10, we fix κ to explore the full behavior of the system. As the signal's energy or frequency increases, the resulting increase in maximum amplitude c affects the Nyquist condition in (5). To maintain a sufficient and comparable number of samples across these conditions, we vary the threshold δ. To ensure

a fair comparison between IF-TEM and classical ADC sampling, all simulations in Figures (8)-(10) were conducted under matched bit budgets and controlled sample counts.

An illustration of the effectiveness of the chosen IF-TEM parameters in reducing the MSE compared to the classical sampler while maintaining constant oversampling is shown in Fig. 8. The analysis focuses on a BL signal $x(t)$ with bandwidth 2Ω, which is constrained in time such that $|x(t)| \leq c$. Here, c is defined as $\sqrt{(E\Omega)/\pi}$, where E ranges from 2 to 10, and the frequency Ω varies between 5 and 100 Hz. The number of bits $N = 8$. IF-TEM method employs fixed values of $\kappa = 0.4$ and $\alpha = b/c = 10$. The threshold δ is chosen to satisfy the condition in equation (37), resulting in an oversampling factor of 4.4. In this scenario, IF-TEM method yields an MSE that is 5 dB lower than that of the conventional method.

Next, by permitting variable oversampling and evaluating the relationship in (4), as represented in Fig. 9, we demonstrate that as the signal energy grows, using IF-TEM sampler, the signal MSE drops. It is noteworthy that this relationship holds for the IF-TEM sampler, but not for the classical sampler, as can be seen from the figure.

Drawing from Theorem 1, our analysis reveals an inverse relationship between signal energy and quantization step size. This reduction in step size leads to potential improvements in the reconstructed signal's MSE. As illustrated in Fig. 9, this phenomenon manifests as a decrease in MSE corresponding to higher signal energy levels. For the IF-TEM implementation, we establish the following parameter configuration: we implement constant values of $\kappa = 2$ and $\alpha = \frac{b}{c} = 5$. To ensure adequate sampling for signal recovery, we select the δ threshold in accordance with the constraint specified in (37). Here, $E \in [2, 10]$, Ω vary from $5 - 100$ Hz, and the number of bits $N = 8$. As demonstrated, up to $E = 4$, the classical sampler yields a lower MSE than the IF-TEM sampler. For $E > 4$, the IF-TEM MSE becomes lower than that of the conventional sampler.

Subsequently, we will prove a sufficient condition for the IF-TEM method to achieve a lower MSE than the classical ADC for the ratio of the IF-TEM bias b to the amplitude bound c. The theorem below provides a summary of this result.

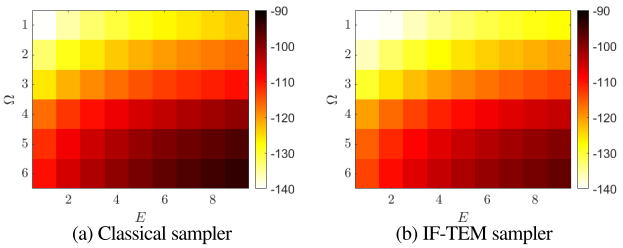

(a) Classical sampler (b) IF-TEM sampler

FIGURE 8. Simulated MSE comparison between (a) classical sampler and (b) IF-TEM ADC with constant oversampling. The MSE of IF-TEM is 8dB lower compared with that of the classical sampler.

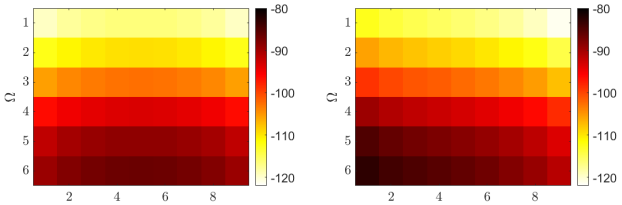

(a) Classical sampler (b) IF-TEM sampler

FIGURE 9. A comparison of simulated MSE between the classical and IF-TEM samplers with a varying oversampling. With the increase of energy, the IF-TEM sampler has lower error compared to with the classical sampler.

Theorem 4: Let $x(t)$, $t \in \mathbb{R}$ be a signal BL to $[-\Omega, \Omega]$. Let E be the maximal energy of $x(t)$, and let the relationship between E, Ω and c be given by $c = \sqrt{E\Omega/\pi}$. Let $\alpha = \frac{b}{c} > 1$, where b is the IF-TEM bias. The IF-TEM achieves a lower MSE than the classical ADC if

$$(\alpha > 1) \quad \text{and} \quad \left(\alpha \leq \left(3 + \beta - \sqrt{\beta^2 + 6\beta + 6}\right)\right) \quad \text{or} \quad \left(\alpha \geq \left(3 + \beta + \sqrt{\beta^2 + 6\beta + 6}\right)\right), \tag{39}$$

where $\beta = \kappa\delta\sqrt{\frac{\Omega}{E\pi}}$.

Proof: See Appendix E. □

Moreover, the condition in Theorem 4 is sufficient but not a necessary condition. Note the conditions $\alpha > 1$ with $\left(\alpha \geq \left(3 + \beta + \sqrt{\beta^2 + 6\beta + 6}\right)\right)$ always yields a possible selection of α resulting in the IF-TEM achieving a lower MSE than the classical ADC. A key insight emerges from examining how this sufficient condition not only influences the bias selection but also affects the IF-TEM's sampling rate. This relationship becomes particularly noteworthy when considering the Nyquist criterion $R = \left(\frac{\kappa\delta}{\alpha - 1}\right)\sqrt{\frac{\Omega}{E\pi}} < 1$. To optimize performance near the Nyquist rate (where $R \approx 1$), the IF-TEM parameters κ, δ are selected to satisfy $\kappa\delta \approx \sqrt{\frac{E\pi}{\Omega}}(\alpha - 1)$. Importantly, although larger values of α may suggest higher oversampling, equations (32)–(33) show that the firing rate F_R is also inversely proportional to δ. Thus, by increasing δ, the oversampling factor can be reduced to practical levels. In our simulations (Figs. 8–10), we maintained OS ≤ 6 even with α =8–10 by fixing κ and adjusting δ accordingly, consistent with hardware constraints where κ is fixed and δ provides the practical degree of freedom.

Fig. 10 presents an empirical comparison between IF-TEM sampler and the classical sampler satisfying the conditions outlined in Theorem 4. The maximal signals amplitude c is defined in (13), $\Omega \in \{5, 10, 20, 50, 80, 100\}$, and $E \in [1, 10]$ satisfy (4). The parameters $\{\kappa, \delta\}$ are chosen as $\kappa = 0.6$ and δ varying between $(0.6, 6)$. The bias b is chosen as $b = \alpha c$, where $\alpha = 8$. Both the IF-TEM and classical sampler

employ an equal number of $N = 12$ bits and an identical total number of samples and the same number of samples in each comparison. For IF-TEM, the actual number of samples varies with frequency and energy, resulting in oversampling factors that naturally grow but remain below 6. It is observed that the MSE decreases as the frequency and energy of the signal increase for the IF-TEM sampler, while there is no such trend for the classical sampler.

In the next section, we show that similar observations are true for the class of FRI signals.

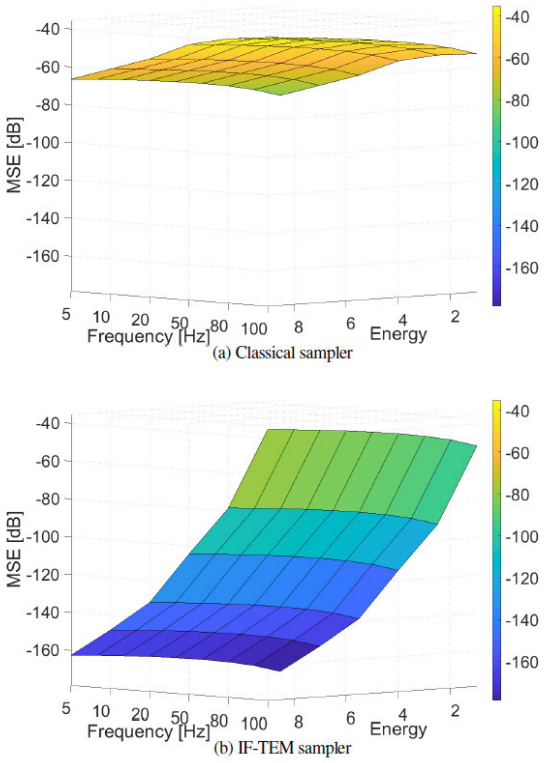

FIGURE 10. Comparison of simulated MSE between (a) classical sampler and (b) IF-TEM ADC using 12 bits.

V. IF-TEM FOR FRI SIGNALS

In this section, we analyze quantization strategies for both conventional and IF-TEM sampling methods when applied to FRI signals. We emphasize that the following discussion of FRI signals is presented at a higher conceptual level than the BL case. Unlike the bandlimited case where we derive formal MSE bounds (Theorems 2-4), our FRI analysis focuses on demonstrating that the key quantization principles extend to this signal class through empirical validation. A complete theoretical characterization of FRI quantization bounds remains valuable future work. Our goal here is not to provide a full derivation of MSE bounds, but rather to illustrate that the quantization principles and performance trends established for BL signals extend naturally to FRI models as well. Our analysis reveals that as we expand the number of pulses L, we observe a corresponding decrease in the sample-wise dynamic range. This finding indicates that quantizer resolution needs to be modified to account for variations in L.

The quantization process mirrors that of BL signals, employing a uniform scalar quantizer with $\log_2 K$ bits of resolution, which generates K discrete output levels. Since the SoS filter has bounded output, the input signal $y(t)$ to the sampler must also remain bounded [34], [37].

$$|y(t)| \leq c = L\ a_{\max}\ \|g\|_\infty \|h\|_1. \tag{40}$$

In the IF-TEM sampling approach, we perform quantization on the temporal differences T_n, with the step size determined by (16). Successfully reconstructing FRI signals from IF-TEM samples requires a minimum of $N \geq 2L + 2$ samples, as shown in (12). To accommodate larger values of L, one can either elevate the bias b or reduce the threshold δ to ensure sufficient samples for accurate reconstruction. To examine how L affects $\Delta_{\text{IF-TEM}}$, we maintain constant values for δ and κ while varying b. Our analysis reveals that $\Delta_{\text{IF-TEM}}$ exhibits an inverse relationship with L, decreasing as L increases. The following theorem formalizes this relationship.

Theorem 5: Consider an IF-TEM sampler coupled with a uniform quantizer operating at K distinct levels with N bits, i.e., $K = 2^N$. Given a fixed $\alpha > 1$, let the IF-TEM bias be represented by b, such that $b = \alpha c$, where c denotes the maximal signal amplitude. For FRI signals, an increase in the number of input pulses L leads to a reduction in the quantization step $\Delta_{\text{IF-TEM}}$.

Proof: Consider fixed values of κ and δ. We select the bias term as $b = \alpha c$ where $\alpha > 1$ is constant. Substituting b into (16), we have

$$\Delta_{\text{IF-TEM}} = \frac{\kappa\delta}{(\alpha+1)(\alpha-1)}\frac{2}{cK}. \tag{41}$$

Based on conditions specified in (12) and (40), when the number of input pulses L grows larger, a reduction occurs in the IF-TEM quantization interval. □

For both IF-TEM and traditional approaches, a higher pulse count L in FRI signals leads to increased sample numbers N when K remains constant. This results in greater total bit counts for both methods.

FRI signals are characterized by L innovations within each time period T, whereas BL signals contain a single innovation ($L = 1$) per Nyquist interval $T = \frac{1}{f_{nyq}} = \frac{\pi}{\Omega}$. Elevating $\Omega > 0$ shortens T, creating an effect similar to increasing L by reducing the quantization interval. This compression of time leads to decreased T_n values. Consequently, based on dense quantization, the quantization error can be reduced, with the IF-TEM method achieving superior performance (lower quantization error) compared to conventional approaches.

Our analysis reveals that significantly exceeding the minimum required sampling rate can negatively affect reconstruction performance. For FRI signals, excessive sampling results in ill-conditioned systems when recovering Fourier coefficients, reducing numerical stability. For BL signals, oversampling leads to longer reconstruction times without

meaningful accuracy improvements. Empirically, we find that an oversampling factor of 2 to 5 times the minimal required rate provides an optimal balance between robustness and efficiency.

In Fig. 11, we experimentally validate the results of Theorem 5. We assess the performance of our proposed IF-TEM quantized sampling approach by measuring MSE and benchmarking it against traditional FRI signal processing methods. Our experiment examines an FRI signal $x(t)$ defined by (9), with a 1-second period T. We test three configurations with $L = 3$, $L = 4$, and $L = 8$ pulses, using 500 random amplitude values between $[-1, 1]$. The temporal locations are randomly distributed in $(0, 1]$ at 0.05 intervals. Both our IF-TEM FRI method and the classical approach employ an SoS sampling kernel to extract $2L$ FSCs [34]. For signals bounded by $|x(t)| \leq c$, with c defined in (40), we configure the IF-TEM parameters as: $b = 10c$, $\delta = 30$, and κ values of 0.5 and 2 for the $L = 3, 4$ and $L = 8$ cases respectively (achieving -98.8 dB error without quantization). We maintain consistent sample counts between IF-TEM and classical methods at approximately $8L$ per measurement. After obtaining the FSCs of $x(t)$, we recover the FRI parameters using orthogonal matching pursuit for both approaches [6]. We evaluate reconstruction quality using the MSE metric:

$$\text{MSE} = \frac{||x(t) - \bar{x}(t)||_{L_2[0,T]}}{||x(t)||_{L_2[0,T]}}, \tag{42}$$

where $\bar{x}(t)$ represents the reconstructed signal.

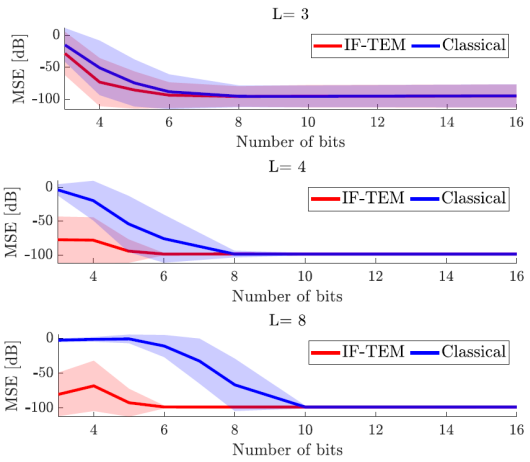

FIGURE 11. Performance analysis of FRI signal estimation across varying bit depths. The plot depicts the average Mean-squared error (solid line) with standard deviation bounds (shaded region) as a function of bit resolution.

Figure 11 displays the MSE comparison between signals reconstructed using the IF-TEM sampling approach (depicted in red) and traditional sampling methods (shown in blue). While IF-TEM quantizes the temporal differences between sampling points, the conventional approach quantizes amplitude values. The analysis maintains consistent sample counts and bit allocation across all data points. The results demonstrate that IF-TEM sampling achieves superior performance, yielding MSE values at least 5dB lower than conventional sampling when utilizing 8 bits or fewer. Both methodologies achieve near-perfect signal reconstruction when employing more than 8 bits. Additionally, the MSE exhibits further improvement as the pulse count L increases or when the innovation rate rises. This relationship mirrors the behavior observed in BL signals, where increasing the input signal frequency produces comparable effects to increasing the pulse count in FRI signals. A comprehensive mathematical analysis comparing the MSE error bounds between quantized IF-TEM sampling and classical uniform sampling for FRI signals lies outside this paper's scope.

VI. CONCLUSION

In this work, we analyzed the effects of quantization on the IF-TEM sampler and demonstrated its advantages over classical ADCs. Specifically, we showed that increasing the bandwidth of a BL signal or the number of pulses of an FRI signal allows reducing the quantization step size when the number of quantization bits is fixed. An upper bound on the signal recovery error was derived for BL signals. Our theoretical and experimental results indicate that, under moderate oversampling (≤ 6) the same number of quantization bits, the IF-TEM sampler with quantized time difference measurements achieves approximately 8 dB lower MSE than uniform samplers with uniform amplitude quantization for both BL and FRI signal models.

APPENDIX

A. PROOF OF LEMMA 1

Let $x(t)$ be a BL signal with bandwidth $[-\Omega, \Omega]$ and maximum amplitude c. Consider an IF-TEM sampler followed by a K-level uniform quantizer with $N = \log_2 K$ bits. The quantization error $d_k = \hat{T}_k - T_k$ is a sequence of uniform i.i.d random variables on $[-\Delta_{\text{IF-TEM}}/2, \Delta_{\text{IF-TEM}}/2]$ The IF-TEM parameters $\{\kappa, b > c, \delta\}$ are chosen to satisfy the Nyquist criterion (5), i.e., $r \triangleq \frac{\kappa\delta\Omega}{\pi(b-c)} < 1$. As a result, the difference between any two consecutive values of the measured time sequence $\{\hat{t}_k\}$ is bounded by the inverse of the Nyquist rate, i.e., $\sup_k \hat{T}_k < T$. Let $w_n(t)$ be defined as

$$w_n(t) = \mathbb{1}_{[-n\Delta t_{\min}, n\Delta t_{\min}]}. \tag{43}$$

In this case, the MSE is calculated using (25) and (27), which yields

$$\begin{aligned}
\varepsilon^2 &= \lim_{n\to\infty} \frac{1}{2n\Delta t_{\min}} ||e\mathbb{1}_{[-n\Delta t_{\min}, n\Delta t_{\min}]}||^2 \\
&= \lim_{n\to\infty} \frac{1}{2n\Delta t_{\min}} || \sum_{k\in Z} (I - \hat{\mathcal{R}})^k \sum_{l\in Z} \epsilon_l \, \text{sinc}_\Omega(t - \hat{s}_l) w_n(t)||^2 \\
&\leq ||\sum_{k\in Z} (I - \hat{\mathcal{R}})^k||^2 \lim_{n\to\infty} \frac{1}{2n\Delta t_{\min}} || \sum_{l\in Z} \epsilon_l \text{sinc}_\Omega(t - \hat{s}_l) w_n(t)||^2 \\
&\leq \frac{1}{(1-r)^2} \lim_{n\to\infty} \frac{1}{2n\Delta t_{\min}} || \sum_{l\in Z} \epsilon_l \, \text{sinc}_\Omega(t - \hat{s}_l) w_n(t)||^2.
\end{aligned} \tag{44}$$

This inequality serves as an upper bound for ε the error signal. Thus, the MSE is upper bounded by

$$\begin{aligned}\mathbb{E}[\varepsilon^2] &\le \mathbb{E}\left[\frac{1}{(1-r)^2}\lim_{n\to\infty}\frac{1}{2n\Delta t_{\min}}\right.\\ &\qquad\left.\times||\sum_{l\in Z}\epsilon_l\,\mathrm{sinc}_\Omega(t-\hat{s}_l)w_n(t)||^2\right]\\ &= \frac{1}{(1-r)^2}\lim_{n\to\infty}\frac{1}{2n\Delta t_{\min}}\\ &\qquad\times\mathbb{E}\left[||\sum_{l\in Z}\epsilon_l\,\mathrm{sinc}_\Omega(t-\hat{s}_l)w_n(t)||^2\right]. \end{aligned}\tag{45}$$

Next, we bound the expectation on the right-hand side as follows

$$\begin{aligned}&\mathbb{E}\left[||\sum_{l\in Z}\epsilon_l\,\mathrm{sinc}_\Omega(t-\hat{s}_l)w_n(t)||^2\right]\\ &=\int_{-n\Delta t_{\min}}^{n\Delta t_{\min}}\sum_{m\in Z}\sum_{k\in Z}\mathrm{sinc}_\Omega(t-\hat{s}_m)\,\mathrm{sinc}_\Omega(t-\hat{s}_k)dt\,\mathbb{E}[\epsilon_k\epsilon_m]\\ &=\int_{-n\Delta t_{\min}}^{n\Delta t_{\min}}\sum_{k\in Z}\mathrm{sinc}_\Omega(t-\hat{s}_k)^2dt\left(\frac{\kappa\delta}{T_k}\right)^2\frac{\Delta^2_{\text{IF-TEM}}}{12}, \end{aligned}\tag{46}$$

where it can be inferred from Appendix B that

$$\mathbb{E}[\epsilon_k\epsilon_m]=\left(\frac{\kappa\delta}{T_k}\right)^2\frac{\Delta^2_{\text{IF-TEM}}}{12}\delta_{k,m}.\tag{47}$$

Given that

$$\Delta t_{\min}=\frac{\kappa\delta}{b+c},\tag{48}$$

we can deduce that

$$\begin{aligned}&\mathbb{E}\left[||\sum_{l\in Z}\epsilon_l\,\mathrm{sinc}_\Omega(t-\hat{s}_l)w_n(t)||^2\right]\\ &\le\int_{-n\Delta t_{\min}}^{n\Delta t_{\min}}\sum_{k\in Z}\mathrm{sinc}_\Omega(t-\hat{s}_k)^2dt\left(\frac{\kappa\delta}{\Delta t_{\min}}\right)^2\frac{\Delta^2_{\text{IF-TEM}}}{12}\\ &=\int_{-n\Delta t_{\min}}^{n\Delta t_{\min}}\sum_{k\in Z}\mathrm{sinc}_\Omega(t-\hat{s}_k)^2dt(b+c)^2\frac{\Delta^2_{\text{IF-TEM}}}{12}. \end{aligned}\tag{49}$$

Furthermore, as given in [16, Result 3]:

$$\frac{1}{2n}\int_{-n\Delta t_{\min}}^{n\Delta t_{\min}}\sum_{k\in Z}\mathrm{sinc}_\Omega(t-\hat{s}_k)^2dt\le\frac{1}{T},\tag{50}$$

where the $T=\frac{\pi}{\Omega}$. Therefore,

$$\mathbb{E}\left[||\sum_{l\in Z}\epsilon_l\,\mathrm{sinc}_\Omega(t-\hat{s}_l)w_n(t)||^2\right]\le\frac{2n}{T}(b+c)^2\frac{\Delta^2_{\text{IF-TEM}}}{12}.\tag{51}$$

Using (45), (48) and (51) results

$$\begin{aligned}\mathbb{E}[\varepsilon^2]&\le\frac{1}{(1-r)^2}\lim_{n\to\infty}\frac{\mathbb{E}\left[||\sum_{l\in Z}\epsilon_l\,\mathrm{sinc}_\Omega(t-\hat{s}_l)w_n(t)||^2\right]}{2n\Delta t_{\min}}\\ &\le\frac{1}{(1-r)^2}\lim_{n\to\infty}\frac{1}{2n\Delta t_{\min}}\frac{2n}{T}(b+c)^2\frac{\Delta^2_{\text{IF-TEM}}}{12}\\ &\le\left(\frac{b+c}{1-r}\right)^2\left(\frac{b+c}{\kappa\delta T}\right)\frac{\Delta^2_{\text{IF-TEM}}}{12}, \end{aligned}\tag{52}$$

which completes the proof.

B. PROOF OF EQUATION (47)

We start by expressing ϵ_k as

$$\begin{aligned}\epsilon_k&=[\kappa\delta-b\hat{T}_k]-\int_{\hat{t}_k}^{\hat{t}_{k+1}}x(u)\mathrm{d}u\\ &=\int_{t_k}^{t_{k+1}}x(u)du-\int_{\hat{t}_k}^{\hat{t}_{k+1}}x(u)\mathrm{d}u-bd_k, \end{aligned}$$

where $d_k=\hat{T}_k-T_k$. By applying the mean-value theorem, we obtain

$$\epsilon_k=x(\zeta_k)T_k-x(\hat{\zeta}_k)\hat{T}_k-bd_k,\tag{53}$$

where $\zeta_k\in(t_k,t_{k+1})$ and $\hat{\zeta}_k\in(\hat{t}_k,\hat{t}_{k+1})$. Note that the quantized IF-TEM values are denoted as $\hat{T}_k=T_k+d_k$, where d_k is the quantization error, The recovered time encodings $\hat{t}_k$ can be expressed as $\hat{t}_k=\sum_{i=1}^k\hat{T}_i=\sum_{i=1}^kT_i+\sum_{i=1}^kd_i$. Assuming that d_k uniform i.i.d random variables on $[-\Delta_{\text{IF-TEM}}/2,\Delta_{\text{IF-TEM}}/2]$, the variance of the error in $\hat{t}_k$ grows with k, given by, $\mathrm{Var}(t_k-\hat{t}_k)=\frac{k\Delta^2_{\text{IF-TEM}}}{12}$. This implies that the errors propagate to later measurements. However, relying on Appendix C, we can choose $\Delta_{\text{IF-TEM}}$ to be sufficiently small such that the following term is finite and bounded

$$\max|t_k-\hat{t}_k|\le\frac{k\Delta_{\text{IF-TEM}}}{2}.\tag{54}$$

Hence, the variance of the difference between t_k and $\hat{t}_k$ remains bounded, demonstrating its non-explosive nature. In particular, this property holds for any $\zeta_k\in(t_k,t_{k+1})$, as the signal $x(t)$ exhibits continuity. By leveraging the continuity property, we can approximate $\zeta_k\approx\hat{\zeta}_k$.

Let us denote a_n to be

$$\begin{aligned}a_n=&\frac{1}{(1-r)^2}\lim_{n\to\infty}\frac{1}{2n\Delta t_{\min}}\\ &\cdot\mathbb{E}\left[||\sum_{l\in Z}\epsilon_l\,\mathrm{sinc}_\Omega(t-\hat{s}_l)w_n(t)||^2\right]. \end{aligned}\tag{55}$$

We show in Appendix C that

$$\lim_{n\to\infty}\frac{1}{2n\Delta t_{\min}}||\sum_{l\in Z}\epsilon_l\,\mathrm{sinc}_\Omega(t-\hat{s}_l)w_n(t)||^2\tag{56}$$

converges. According to the definition of the limit, we have

$$\forall\epsilon>0\exists n'\in\mathbb{N}\quad\text{s.t.}\quad-\epsilon\le a_{n'}-\lim_{n\to\infty}a_n\le\epsilon\tag{57}$$

since $\mathbb{E}[\varepsilon^2]\le\lim_{n\to\infty}a_n\le a_{n'}+\epsilon$.

Using this n', we can choose $\Delta_{\text{IF-TEM}}$ to be sufficiently small such that

$$\max_k |t_k - \hat{t}_k| \leq \frac{k\Delta_{\text{IF-TEM}}}{2} \leq \frac{(2n'+1)\Delta_{\text{IF-TEM}}}{2}. \quad (58)$$

This implies that in this case, $\zeta_k \approx \hat{\zeta}_k$, and we can approximate ϵ_k as $\epsilon_k \approx (-x(\zeta_k) - b)\, d_k$.

Since

$$x(\zeta_k) = \frac{1}{T_k}\int_{t_k}^{t_{k+1}} x(u)du = -b + \frac{\kappa\delta}{T_k}, \quad (59)$$

we have $\epsilon_k \approx \frac{\kappa\delta}{T_k} d_k$. Therefore,

$$\mathbb{E}[\epsilon_k \epsilon_m] = \frac{\kappa\delta}{T_k}\frac{\kappa\delta}{T_m}\mathbb{E}[d_k d_m] = \left(\frac{\kappa\delta}{T_k}\right)^2 \frac{\Delta^2_{\text{IF-TEM}}}{12}\delta_{k,m}, \quad (60)$$

which completes the proof.

C. PROOF OF THE CONVERGENCE OF (56)

To prove convergence of (56), we first consider the boundedness and increasing nature of the term

$$\mathbb{E}\left[\left|\left|\sum_{l\in Z}\epsilon_l \operatorname{sinc}_\Omega(t-\hat{s}_l)w_n(t)\right|\right|^2\right]. \quad (61)$$

We begin by demonstrating the boundedness of this term

$$\begin{aligned}
&\mathbb{E}\left[\left|\left|\sum_{l\in Z}\epsilon_l \operatorname{sinc}_\Omega(t-\hat{s}_l)w_n(t)\right|\right|^2\right] \\
&\leq \mathbb{E}\left[\sum_{l\in Z}|\epsilon_l|^2\left|\left|\operatorname{sinc}_\Omega(t-\hat{s}_l)w_n(t)\right|\right|^2\right] \\
&\leq \max_l |\epsilon_l|^2\left[\sum_{l\in Z}\mathbb{E}\left|\left|\operatorname{sinc}_\Omega(t-\hat{s}_l)w_n(t)\right|\right|^2\right] \\
&\leq \max_l |\epsilon_l|^2 ||\operatorname{sinc}_\Omega(t)||_2^2 |\#l|, \quad (62)
\end{aligned}$$

where we note that as shown in Appendix D ϵ_l is bounded, and $|\#l|$ is the number of spikes (time instances) in the window. Note that the number of spikes in a window in $[-n\Delta t_{\min}, n\Delta t_{\min}]$, is upper bounded by $\frac{2n\Delta t_{\min}}{\Delta t_{\min}} + 1 = 2n+1$. Thus, we have

$$|\#l| \leq 2n+1. \quad (63)$$

and consequently,

$$\begin{aligned}
&\mathbb{E}\left[\left|\left|\sum_{l\in Z}\epsilon_l \operatorname{sinc}_\Omega(t-\hat{s}_l)w_n(t)\right|\right|^2\right] \\
&\leq \left(\kappa\delta + (b+c)\left(\Delta t_{\max} + \frac{\Delta_{\text{IF-TEM}}}{2}\right)\right)^2 \\
&\quad \times ||\operatorname{sinc}_\Omega(t)||_2^2 (2n+1). \quad (64)
\end{aligned}$$

Moreover, the above norm is shown to be increasing in n [16]. Dividing $\mathbb{E}\left[\left|\left|\sum_{l\in Z}\epsilon_l \operatorname{sinc}_\Omega(t-\hat{s}_l)w_n(t)\right|\right|^2\right]$ by the window size $2n\Delta t_{\min}$, we find that its upper bound is a constant. Therefore, we have established that the following term converges:

$$\lim_{n\to\infty}\frac{1}{2n\Delta t_{\min}}\left|\left|\sum_{l\in Z}\epsilon_l \operatorname{sinc}_\Omega(t-\hat{s}_l)w_n(t)\right|\right|^2,$$

which completes the proof.

D. PROOF OF BOUNDEDNESS OF (26)

Here we establish the boundedness of ϵ_l as defined in (26). Taking into account the definition provided in (26), we prove that ϵ_l is bounded. The bound on the absolute value of ϵ_l is evaluated as

$$\begin{aligned}
|\epsilon_l| &= \left|[\kappa\delta - b\hat{T}_l] - \int_{\hat{t}_l}^{\hat{t}_{l+1}} x(u)\mathrm{d}u\right| \\
&\leq \kappa\delta + b|\hat{T}_l| + \left|\int_{\hat{t}_l}^{\hat{t}_{l+1}} x(u)\mathrm{d}u\right|. \quad (65)
\end{aligned}$$

Considering that $\hat{T}_l = T_l + d_l$, where $\Delta t_{\min} \leq T_l \leq \Delta t_{\max}$ and the quantization error $d_l \in [-\frac{\Delta_{\text{IF-TEM}}}{2}, \frac{\Delta_{\text{IF-TEM}}}{2}]$, we can derive

$$|\hat{T}_l| \leq |T_l| + |d_l| \leq \Delta t_{\max} + \frac{\Delta_{\text{IF-TEM}}}{2}. \quad (66)$$

Furthermore, employing the mean-value theorem, the integral term can be expressed as

$$\begin{aligned}
\left|\int_{\hat{t}_l}^{\hat{t}_{l+1}} x(u)\mathrm{d}u\right| &= |x(\zeta_l)||\hat{t}_{l+1} - \hat{t}_l| \\
&\leq c|\hat{T}_l| \leq c\left(\Delta t_{\max} + \frac{\Delta_{\text{IF-TEM}}}{2}\right), \quad (67)
\end{aligned}$$

where $\zeta_l \in (\hat{t}_l, \hat{t}_{l+1})$ and $x(t) \leq c$. Hence, by applying (67) in (65), we can conclude that

$$|\epsilon_l| \leq \kappa\delta + (b+c)\left(\Delta t_{\max} + \frac{\Delta_{\text{IF-TEM}}}{2}\right), \quad (68)$$

which completes the proof.

E. PROOF OF THEOREM 4

Based on Theorem 3, we can deduce that $0 < R < 1$ and that $\left(\frac{1}{2(1-R)^2}\right)\left(\frac{\alpha+1}{\alpha-1}\right)^2 \leq 1$, where $\alpha = \frac{b}{c} > 1$, and $R = \left(\frac{\kappa\delta}{\alpha-1}\right)\sqrt{\frac{\Omega}{E\pi}} < 1$. This inequality holds if and only if $0 < R < 1$ and $(1-R)^2 \geq \frac{1}{2}\left(\frac{\alpha+1}{\alpha-1}\right)^2$. Let us denote $\beta = \frac{1}{2}\left(\frac{\alpha+1}{\alpha-1}\right)^2$. Then, the inequality holds if and only if $0 < R < 1$ and $(1-R \geq \beta$ or $1-R \leq -\beta)$. Using the distributive law, this can be simplified to

$$0 < R < 1 \quad \text{and} \quad ((1-R \geq \beta) \quad \text{or} \quad (1-R \leq -\beta)). \quad (69)$$

Since $\alpha > 1$, we can deduce that $\beta > 0$. Therefore, the case where $0 < R < 1$ and $1 + \beta \leq R$ is not possible. Thus, the inequality holds if and only if $0 < R < 1$ and $(1 - \beta \geq R)$.

Given the definitions of $R = \left(\frac{\kappa\delta}{\alpha-1}\right)\sqrt{\frac{\Omega}{E\pi}}$ and β, solving the quadratic equation $(1-\beta > R)$ for α yields

$$\left(\alpha \leq \left(3+t-\sqrt{t^2+6t+6}\right)\right) \quad \text{or} \quad \left(\alpha \geq \left(3+t+\sqrt{t^2+6t+6}\right)\right), \tag{70}$$

where $t = \kappa\delta\sqrt{\frac{\Omega}{E\pi}}$ and $\alpha > 1$. Therefore, we have shown that the upper bound for the IF-TEM MSE outperforms that of the classical ADC when (70) holds. Thereby indicating that the IF-TEM achieves superior MSE performance compared to the classical ADC in such instances This completed the theorem proof.

ACKNOWLEDGMENT

Hila Naaman has conducted this research as a Ph.D. Student at the Weizmann Institute of Science under the supervision of Prof. Y. C. Eldar. An earlier version of this paper was presented in part at the European Signal Processing Conference (EUSIPCO), in September 2022 [1].

REFERENCES

[1] H. Naaman, S. Mulleti, Y. C. Eldar, and A. Cohen, "Time-based quantization for FRI and bandlimited signals," in *Proc. 30th Eur. Signal Process. Conf. (EUSIPCO)*, Aug. 2022, pp. 2241–2245.
[2] S. V. Vaseghi, *Advanced Digital Signal Processing and Noise Reduction*. Hoboken, NJ, USA: Wiley, 2008.
[3] T. Berger and J. D. Gibson, "Lossy source coding," *IEEE Trans. Inf. Theory*, vol. 44, no. 6, pp. 2693–2723, Oct. 1998.
[4] Z. Fang, L. Lou, K. Tang, W. Wang, B. Chen, Y. Wang, and Y. Zheng, "A CMOS-integrated radar-assisted cognitive sensing platform for seamless human–robot interactions," in *Proc. IEEE Int. Symp. Circuits Syst. (ISCAS)*, May 2021, pp. 1–4.
[5] H. Nyquist, "Certain topics in telegraph transmission theory," *Trans. Amer. Inst. Electr. Eng.*, vol. 47, no. 2, pp. 617–644, Apr. 1928.
[6] Y. C. Eldar, *Sampling Theory: Beyond Bandlimited Systems*. Cambridge, U.K.: Cambridge Univ. Press, 2015.
[7] M. Miśkowicz and D. Kościelnik, "The dynamic range of timing measurements of the asynchronous sigma-delta modulator," *IFAC Proc. Volumes*, vol. 39, no. 21, pp. 395–400, Feb. 2006.
[8] D. Koscielnik and M. Miskowicz, "Designing time-to-digital converter for asynchronous ADCs," in *Proc. IEEE Design Diag. Electron. Circuits Syst.*, May 2007, pp. 1–6.
[9] H. Naaman, S. Mulleti, and Y. C. Eldar, "Uniqueness and robustness of tem-based FRI sampling," in *Proc. IEEE Int. Symp. Inf. Theory (ISIT)*, Jun. 2022, pp. 2631–2636.
[10] S. Mulleti, T. Zirtiloglu, A. Tan, R. T. Yazicigil, and Y. C. Eldar, "Power-efficient sampling," 2023, *arXiv:2312.10966*.
[11] S. Mulleti, A. Bhandari, and Y. C. Eldar, "Power-aware analog to digital converters," in *Sampling*, Jun. 2024, pp. 415–452.
[12] M. Miśkowicz, *Event-Based Control and Signal Processing*. Boca Raton, FL, USA: CRC Press, 2018.
[13] E. Allier, G. Sicard, L. Fesquet, and M. Renaudin, "A new class of asynchronous A/D converters based on time quantization," in *Proc. 9th Int. Symp. Asynchronous Circuits Syst.*, 2003, pp. 196–205.
[14] E. Roza, "Analog-to-digital conversion via duty-cycle modulation," *IEEE Trans. Circuits Syst. II, Analog Digit. Signal Process.*, vol. 44, no. 11, pp. 907–914, Nov. 2022.
[15] H. G. Feichtinger, J. C. Príncipe, J. L. Romero, A. Singh Alvarado, and G. A. Velasco, "Approximate reconstruction of bandlimited functions for the integrate and fire sampler," *Adv. Comput. Math.*, vol. 36, no. 1, pp. 67–78, Jan. 2012.
[16] A. A. Lazar and L. T. Toth, "Perfect recovery and sensitivity analysis of time encoded bandlimited signals," *IEEE Trans. Circuits Syst. I, Reg. Papers*, vol. 51, no. 10, pp. 2060–2073, Oct. 2004.
[17] A. A. Lazar and L. T. Toth, "Time encoding and perfect recovery of bandlimited signals," in *Proc. IEEE Int. Conf. Acoust., Speech, Signal Process. (ICASSP)*., vol. 1, Apr. 2003, pp. 709-712.
[18] A. Lazar, "Time encoding with an integrate-and-fire neuron with a refractory period," *Neurocomputing*, vols. 58–60, pp. 53–58, Jun. 2004.
[19] M. Rastogi, A. S. Alvarado, J. G. Harris, and J. C. Príncipe, "Integrate and fire circuit as an ADC replacement," in *Proc. IEEE Int. Symp. Circuits Syst. (ISCAS)*, May 2011, pp. 2421–2424.
[20] S. Ryu, C. Y. Park, W. Kim, S. Son, and J. Kim, "A time-based pipelined ADC using integrate-and-fire multiplying-DAC," *IEEE Trans. Circuits Syst. I, Reg. Papers*, vol. 68, no. 7, pp. 2876–2889, Jul. 2021.
[21] H. Naaman, N. Glazer, M. Namer, D. Bilik, S. Savariego, and Y. C. Eldar, "Hardware prototype of a time-encoding sub-Nyquist ADC," *IEEE Trans. Instrum. Meas.*, vol. 73, pp. 1–13, 2024.
[22] B. Rajendran, A. Sebastian, M. Schmuker, N. Srinivasa, and E. Eleftheriou, "Low-power neuromorphic hardware for signal processing applications: A review of architectural and system-level design approaches," *IEEE Signal Process. Mag.*, vol. 36, no. 6, pp. 97–110, Nov. 2019.
[23] F. Barranco, C. Fermüller, and Y. Aloimonos, "Contour motion estimation for asynchronous event-driven cameras," *Proc. IEEE*, vol. 102, no. 10, pp. 1537–1556, Oct. 2014.
[24] H. Naaman, D. Bilik, S. Savariego, M. Namer, and Y. C. Eldar, "ECG-TEM: Time-based sub-Nyquist sampling for ECG signal reconstruction and hardware prototype," 2024, *arXiv:2405.13904*.
[25] A. A. Lazar and E. A. Pnevmatikakis, "Video time encoding machines," *IEEE Trans. Neural Netw.*, vol. 22, no. 3, pp. 461–473, Mar. 2011.
[26] K. Adam, A. Scholefield, and M. Vetterli, "Sampling and reconstruction of bandlimited signals with multi-channel time encoding," *IEEE Trans. Signal Process.*, vol. 68, pp. 1105–1119, 2020.
[27] N. T. Thao and D. Rzepka, "Time encoding of bandlimited signals: Reconstruction by pseudo-inversion and time-varying multiplierless FIR filtering," *IEEE Trans. Signal Process.*, vol. 69, pp. 341–356, 2021.
[28] K. Adam, A. Scholefield, and M. Vetterli, "Asynchrony increases efficiency: Time encoding of videos and low-rank signals," *IEEE Trans. Signal Process.*, vol. 70, pp. 105–116, 2022.
[29] D. Gontier and M. Vetterli, "Sampling based on timing: Time encoding machines on shift-invariant subspaces," *Appl. Comput. Harmon. Anal.*, vol. 36, no. 1, pp. 63–78, Jan. 2014.
[30] A. Aldroubi and K. Gröchenig, "Nonuniform sampling and reconstruction in shift-invariant spaces," *SIAM Rev.*, vol. 43, no. 4, pp. 585–620, Jan. 2001.
[31] E. A. Pnevmatikakis, *Spikes As Projections: Representation and Processing of Sensory Stimuli in the Time Domain*. New York, NY, USA: Columbia Univ. Press, 2010.
[32] R. Alexandru and P. L. Dragotti, "Reconstructing classes of non-bandlimited signals from time encoded information," *IEEE Trans. Signal Process.*, vol. 68, pp. 747–763, Feb. 2019.
[33] S. Rudresh, A. J. Kamath, and C. S. Seelamantula, "A time-based sampling framework for finite-rate-of-innovation signals," in *Proc. IEEE Int. Conf. Acoust., Speech Signal Process. (ICASSP)*, May 2020, pp. 5585–5589.
[34] H. Naaman, S. Mulleti, and Y. C. Eldar, "FRI-TEM: Time encoding sampling of finite-rate-of-innovation signals," *IEEE Trans. Signal Process.*, vol. 70, pp. 2267–2279, 2022.
[35] H. Naaman, E. Reznitskiy, N. Glazer, M. Namer, and Y. C. Eldar, "Sub-Nyquist time-based sampling of FRI signals," in *Proc. IEEE Int. Conf. Acoust., Speech Signal Process. (ICASSP)*, Jun. 2021.
[36] A. J. Kamath, S. Rudresh, and C. S. Seelamantula, "Time encoding of finite-rate-of-innovation signals," 2021, *arXiv:2107.03344*.
[37] A. Papoulis, "Limits on bandlimited signals," *Proc. IEEE*, vol. 55, no. 10, pp. 1677–1686, 1967.
[38] M. Vetterli, P. Marziliano, and T. Blu, "Sampling signals with finite rate of innovation," *IEEE Trans. Signal Process.*, vol. 50, no. 6, pp. 1417–1428, Jun. 2002.
[39] R. Tur, Y. C. Eldar, and Z. Friedman, "Innovation rate sampling of pulse streams with application to ultrasound imaging," *IEEE Trans. Signal Process.*, vol. 59, no. 4, pp. 1827–1842, Apr. 2011.
[40] L. Tan and J. Jiang, *Digital Signal Processing: Fundamentals and Applications*. New York, NY, USA: Academic, 2018.

HILA NAAMAN (Member, IEEE) received the B.Sc. degree in physics and mathematics and the M.Sc. degree in physics from Bar-Ilan University, Israel, in 2012 and 2017, respectively, and the Ph.D. degree from the Mathematics and Computer Science Department, Weizmann Institute of Science, Israel, in 2024, under the supervision of Prof. Yonina Eldar. Currently, she is a Researcher and a Lecturer with the Department of Computer Science, College of Management, Israel. Her research interests include event-based information processing, signal processing and its intersection with machine learning and data science, and sampling theory and its applications.

NEIL IRWIN BERNARDO (Member, IEEE) received the Bachelor of Science degree in electronics and communications engineering and the Master of Science degree in electrical engineering from the University of the Philippines Diliman, in 2014 and 2016, respectively, and the Doctor of Philosophy degree in engineering from the University of Melbourne, Australia. He is currently an Associate Professor with the Electrical and Electronics Engineering Institute, University of the Philippines Diliman. His research interests include wireless communications, signal processing, and information theory.

ALEJANDRO COHEN (Senior Member, IEEE) received the M.Sc. and Ph.D. degrees from the Department of Communication Systems Engineering, Ben-Gurion University of the Negev, Be'er Sheva, Israel, in 2013 and 2018, respectively. He is currently an Assistant Professor with the Faculty of Electrical and Computer Engineering, Technion, Haifa, Israel. From 2019 to 2021, he was a Senior Postdoctoral Associate with the Department of Electrical Engineering and Computer Science, Massachusetts Institute of Technology, Cambridge, MA, USA. From 2007 to 2014, he was with the DSP Group, where he worked on voice enhancement and signal processing. From 2014 to 2019, he was with Intel, Santa Clara, CA, USA, where he was a Research Scientist with the Innovation Group at Mobile and Wireless. His research interests include information theory, signal processing and networks, wireless communication, security, post-quantum cryptography, network information theory and network coding, coding, computation in networks, and speech enhancement.

YONINA C. ELDAR (Fellow, IEEE) received the B.Sc. degree in physics and the B.Sc. degree in electrical engineering from Tel-Aviv University, and the Ph.D. degree in electrical engineering and computer science from MIT, in 2002. She is a Professor with the Department of Mathematics and Computer Science, Weizmann Institute of Science, Rehovot, Israel, where she heads the Center for Biomedical Engineering and Signal Processing and holds the Dorothy and Patrick Gorman Professorial Chair. She is also a Visiting Professor with MIT, a Visiting Scientist with the Broad Institute, and an Adjunct Professor with Duke University. She was a Visiting Professor with Stanford. She is a member of Israel Academy of Sciences and Humanities and a EURASIP Fellow. She was an Horev Fellow of the Leaders in Science and Technology Program at Technion and an Alon Fellow. She has received many awards for excellence in research and teaching, including the IEEE Signal Processing Society Technical Achievement Award, in 2013; the IEEE/AESS Fred Nathanson Memorial Radar Award, in 2014; and the IEEE Kiyo Tomiyasu Award, in 2016. She received the Michael Bruno Memorial Award from the Rothschild Foundation, the Weizmann Prize for Exact Sciences, the Wolf Foundation Krill Prize for Excellence in Scientific Research, the Henry Taub Prize for Excellence in Research (twice), the Hershel Rich Innovation Award (three times), and the Award for Women with Distinguished Contributions. She also received several best paper awards and best demo awards together with her research students and colleagues. She was a recipient of the Israel Prize in Engineering Research. She was selected as one of the 50 most influential women in Israel. She was a member of Israel Committee for Higher Education. She is the Editor-in-Chief of *Foundations and Trends in Signal Processing*, a member of several IEEE technical committees and award committees, and heads the Committee for Promoting Gender Fairness in Higher Education Institutions in Israel.